Marine and Petroleum Geology 97 (2018) 493–516

Contents lists available at ScienceDirect

Marine and Petroleum Geology

journal homepage: www.elsevier.com/locate/marpetgeo

Research paper

Generation, migration, entrapment and leakage of microbial gas in the Dutch part of the Southern North Sea Delta

J.M. Verweij*, S.N. Nelskamp, J.H. Ten Veen, G. De Bruin, K. Geel, T.H. Donders[1]

TNO Netherlands Organisation for Applied Scientific Research, Princetonlaan 6, 3584 CB Utrecht, The Netherlands

ARTICLE INFO

Keywords:
Microbial gas system
Gas generation modelling
Capillary seal capacity
Southern north sea delta

ABSTRACT

Understanding the shallow gas system is critical for assessing its potential as an energy source, for evaluating the possible hazard of shallow gas for drilling and wind farm locations and for evaluating the effect of gas emissions at the seabed on marine ecosystems and climate. This paper presents the key elements and processes of the microbial shallow gas system in the Plio-Pleistocene Dutch Southern North Sea Delta based on recent findings from different projects. Geochemical and carbon isotopic composition of shallow gas occurrences in the delta are indicative of a microbial origin of the gas. Shallow gas mainly occurs in stratigraphic traps and stacked anticlinal structures above salt structures, as indicated by identified direct hydrocarbon indicators on seismic, such as bright spots. Organic matter in the delta deposits is of predominantly land plant origin with TOC values varying between < 1% and 5%, and mostly between 1 and 2%. Simulations of temperature and burial history in combination with dedicated 1D simulations of microbial gas generation reveal that gas generation in the delta started in Early Pleistocene Calabrian times and is still ongoing. Simulated volumes of gas generation are more than enough to fill published estimated volumes of shallow gas prospects in the delta. The geometry of the E-W prograding delta sequences and the close interbedding of interglacial silty/sandy and glacial clayey/silty sediments focus gas migration updip through the foresets towards the topsets of the delta sequences, and ultimately into the anticlinal stacked traps. Grain-size based calculations of the permeability and capillary seal capacity of clayey/silty seals of the stratigraphic and anticlinal traps provided first estimates of permeability values ranging from 2.8E-20 m^2 to 1.1E-18 m^2 and capillary seal capacity values between 10m and 24m. Comparison of gas column heights derived from grain-size based calculations, cross plots of neutron and density logs and pressure measurements, with trap heights derived from seismic bright spots suggests that many traps in stacked bright spots are not filled to structural spill point. This suggests that filling of the stacked reservoirs is not related to fill-spill migration, but rather to leakage through the top seal. In absence of fault and fracture zones crossing the seal, this leakage is related to the capillary seal capacity and permeability of the top seal. The leakage extends, locally, to the seabed.

The microbial gas system in the delta today is a highly dynamic system driven by ongoing burial of the delta sediments and microbial gas generation.

1. Introduction

Shallow gas accumulations concern gas accumulations located at a depth of less than about 1000 m. Worldwide, and also in the Netherlands, increasing attention is focused on shallow gas accumulations and leakage of shallow gas to the seabed for various reasons, including the significance of shallow gas as an important energy resource, as a possible geohazard for drilling and wind farm locations, and the effect of gas emissions at the seabed on marine ecosystems and climate (Gentz, 2013; Judd and Hovland, 2009; Mau et al., 2015; Rollet et al., 2006; Römer et al., 2017; Schroot et al., 2005; Ten Veen et al., 2014; Van den Boogaard et al., 2013).

Several boreholes encountered shallow gas accumulations in Plio-Pleistocene Southern North Sea Delta (SNS delta) deposits in the Dutch northern offshore since the late 1980s (e.g. A12-03, A15-02, A18-02, A18-02S1, B10-03, B13-03, B16-01, B17-05, B17-06, F02-05) (Fig. 1). In addition, indicators of shallow gas and gas leakage in the Dutch northern offshore have been recognized since many years and include subsurface seismic indicators, such as bright spots, flat spots and gas chimneys (Foschi et al., 2018; Kombrink et al., 2012b; Kuhlmann and

* Corresponding author.
E-mail address: hanneke.verweij@outlook.com (J.M. Verweij).
[1] Present address: Department of Physical Geography, Faculty of Geosciences, Utrecht University, Princetonlaan 8a, 3584 CB Utrecht, The Netherlands.

https://doi.org/10.1016/j.marpetgeo.2018.07.034
Received 9 November 2017; Received in revised form 30 July 2018; Accepted 31 July 2018
Available online 01 August 2018

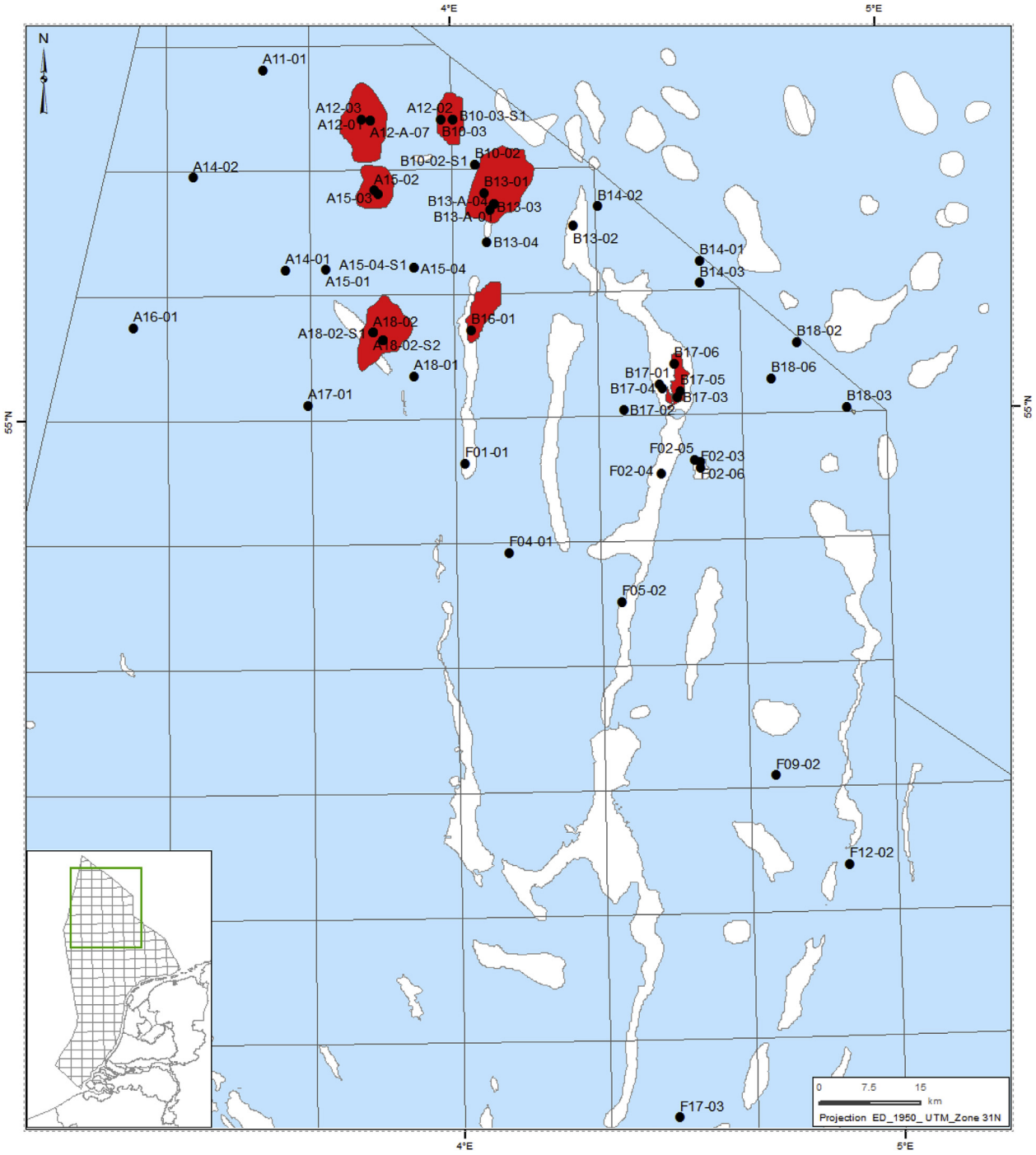

Fig. 1. Location of study area, showing shallow gas accumulations (in red), salt structures (in white) and location of wells. (For interpretation of the references to colour in this figure legend, the reader is referred to the Web version of this article.)

Wong, 2008; Stuart and Huuse, 2012; Ten Veen et al., 2013, 2014; Van den Boogaard and Hoetz, 2012; Williams and Gent, 2015), pockmarks at the seabed (Laban, 1999; Schroot and Schüttenhelm, 2003), and gas emissions from the seabed (Brussaard, 2013; Gentz, 2013; Mau et al., 2015; Römer et al., 2017; Schroot et al., 2005). Inventory of bright spots on seismic data showed that many of the potential gas accumulations occur in stratigraphic traps or in multiple stacked reservoirs in anticlinal traps above salt structures and are sometimes associated with faults (Kombrink et al., 2012b; Kuhlmann and Wong, 2008; Schroot and Schüttenhelm, 2003; Schroot et al., 2005; Ten Veen et al., 2013, 2014; Van den Boogaard and Hoetz, 2012; Williams and Gent, 2015) (Fig. 2). Van den Boogaard et al. (2013) presented a preliminary total volume estimate for the shallow gas play of 36–118 billion cubic metres Gas Initially In Place (bcm GIIP).

The shallow gas fields (Fig. 1) were not developed initially due to the limited strength of the unconsolidated sandy reservoir and the expected early water breakthrough and sand production (Van den Boogaard and Hoetz, 2012). Gas field A12-FA is the first shallow gas field that was taken into production in 2007. This was almost 30 years after borehole A12-03 encountered the shallow gas field A12-FA in 1988. Three other shallow gas fields in the northern offshore are currently in production: the second shallow gas field HANP (also called F02a-Pliocene field) came into production in 2009, followed by field B13-FA in 2011, and field A18-FA in January 2016.

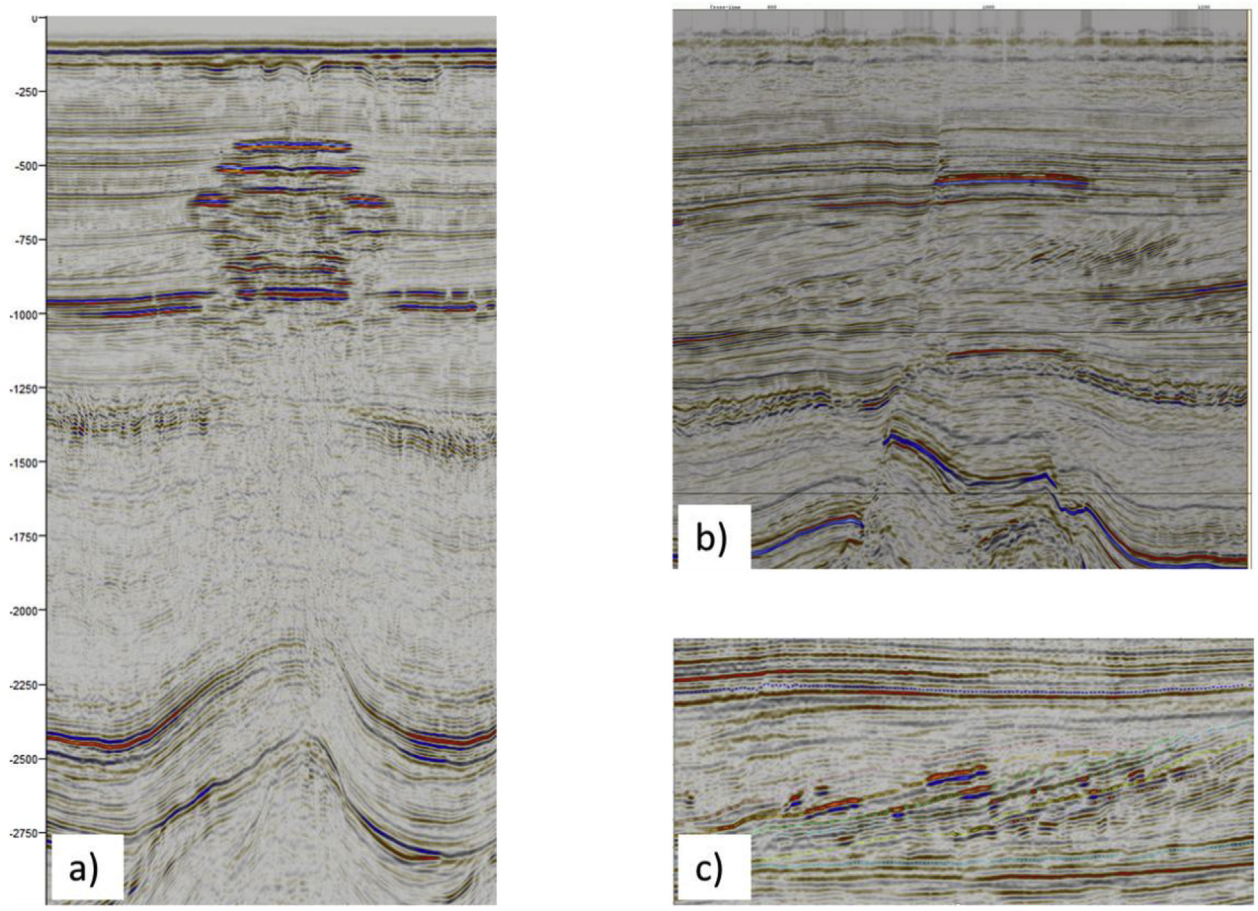

Fig. 2. Examples of seismic indicators of gas occurrences: a) stacked bright spots in 4 way dip closure, b) bright spots related to fault zone, and c) bright spots in delta front sequences.

The start of the successful production of shallow gas fields showed the economic potential of shallow gas in the northern offshore of the Netherlands. This in combination with changing trends in E&P in the Netherlands led to the need for more detailed knowledge and understanding of the shallow gas play. Several projects were initiated for that reason, including a joint industry project in which five major companies operating in the Southern North Sea participated (Ten Veen et al., 2013, 2014), and TNO in-house research projects with special focus on microbial gas generation (Verweij and Nelskamp, 2014), capillary seal capacity of intra-delta mudstone caprocks of shallow gas occurrences (Daza Cajigal, 2012; Verweij et al., 2014) and leakage (Verweij et al., 2015, 2016). The joint industry project involved the development of a multidisciplinary workflow and its application to the SNS delta, including: 1) the reconstruction of the internally complex geological framework of the delta based on sequence stratigraphic/seismic interpretations of key horizons (constrained by biostratigraphic data) and petrophysical data, 2) a combined deterministic/stochastic approach to make reservoir property predictions, 3) classification of acoustic bright spots, 4) evaluation of the origin of shallow gas, and 4) a grain-size based method to estimate the integrity of intra-delta seals.

The focus of this paper is on the key elements and processes of the microbial gas system in the Dutch SNS delta. It is based on new findings from the above mentioned projects combined with existing knowledge and information on the geological, geothermal and pressure and fluid dynamic evolution of the area and relevant well data and information published on the Dutch oil and gas portal (www.nlog.nl).

2. Geological and hydrogeological setting of the Southern North Sea Delta

The Neogene paleo-delta of the Southern North Sea (also known as Eridanos Delta, Overeem et al., 2001) was fed by a fluvio-deltaic system that prograded through Northwestern Europe due to simultaneous uplift and erosion of the Fennoscandinavian Shield and accelerated subsidence of the North Sea Basin. The Dutch part of the SNS delta consists of sedimentary sequences of mostly Plio-Pleistocene age. The overall depositional trend of these Plio-Pleistocene deltaic sequences is an east to west prograding system, which downlaps onto the Mid Miocene Unconformity (Fig. 3). The system is capped by 300–400 m of Upper Pleistocene and Holocene deposits. The present-day base of the delta reaches its greatest depth in the northeasternmost part of the Dutch offshore (Fig. 4).

The Plio-Pleistocene delta is subdivided into 13 sequences (S1 to S13, e.g. Kuhlmann et al., 2004) that are grouped into three main depositional units (Ten Veen et al., 2013), which are strongly affected by paleoclimate that controlled sea level (Kuhlmann et al., 2006a, 2006b), sediment supply and energy regime (Fig. 3):

- Basal depositional unit (sequences S1-S4). This overall shallowing unit was deposited during a period characterized by temperate climate conditions. The basal sequences were deposited in relatively deep water, while the top sequences were deposited in a shallow marine environment. The unit is characterized by steeply dipping clinoforms with high relief; the clinoforms are flatter with less relief in the top sequence which was deposited during the transition from a temperate to a cold climate (S4). The top of the S4 sequence

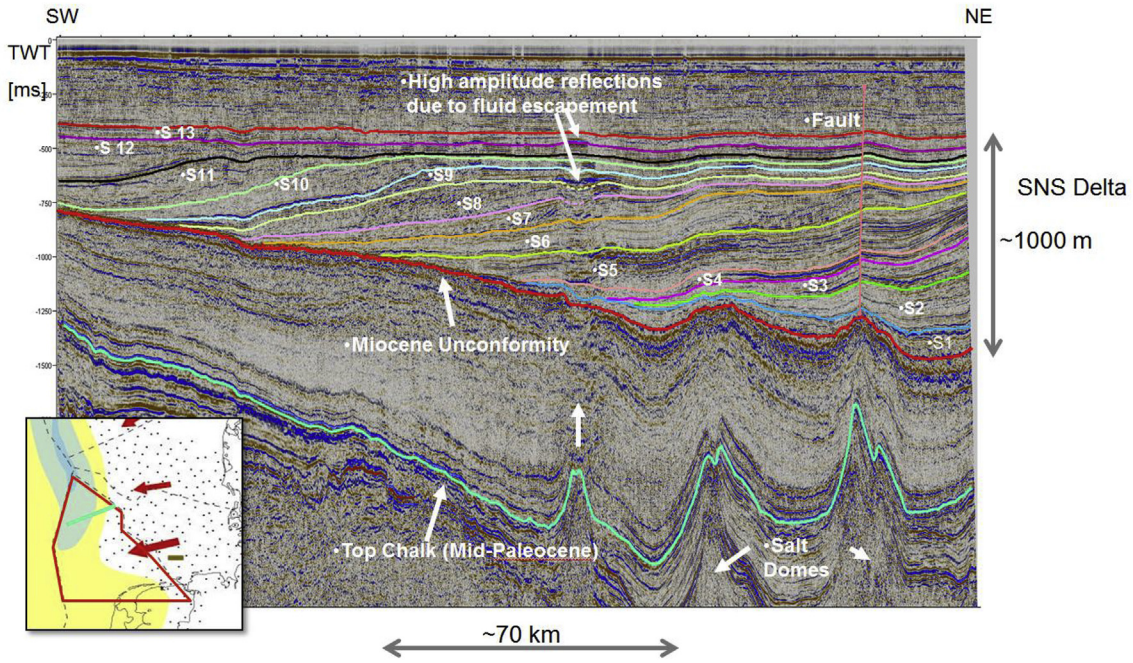

Fig. 3. SW-NE seismic cross section showing the westward prograding Southern North Sea Delta of Plio-Pleistocene age. The delta is subdivided into 13 seismostratigraphic sequences (S1 to S13). The inset shows the location of the cross section in the northern offshore of the Netherlands.

coincides with the Plio-Pleistocene transition.

- Intermediate depositional unit (sequences S5-S7). The alternation of warm and cold periods during deposition of this unit had a strong impact on the development of the delta sequences S5-S7 and the characteristics of its sediments. The glacial-interglacial cycles are associated with differences in grain size, sea surface temperature and climate and are also a key control on the presence and distribution of potentially sealing layers, coarser-grained reservoir layers, as well as distribution of organic matter in the sediments (Donders et al., 2018; Ten Veen et al., 2014) (Fig. 5).
- Top depositional unit (sequences S8-S13). This youngest unit was deposited in a shallow sea under arctic conditions with sea ice cover. Glacial plow marks are a frequent sight. Some of the units represent warmer periods with an open vegetation and more open marine conditions.

The delta is covered with predominantly continental deposits (glacigenic and fluvial deposits) and some marine deposits. Sedimentation rates were high to very high during deposition of the delta sedimentary sequences and continued to be high until present-day (Fig. 6).

After deposition of the delta sediments, i.e. after 1.8 Ma, there were 3 main phases in which ice sheets reached the Dutch North Sea, namely the Elsterian, Saalian and Weichselian phases of glaciation. During the Elsterian, coalescing Scandinavian and British ice sheets covered the

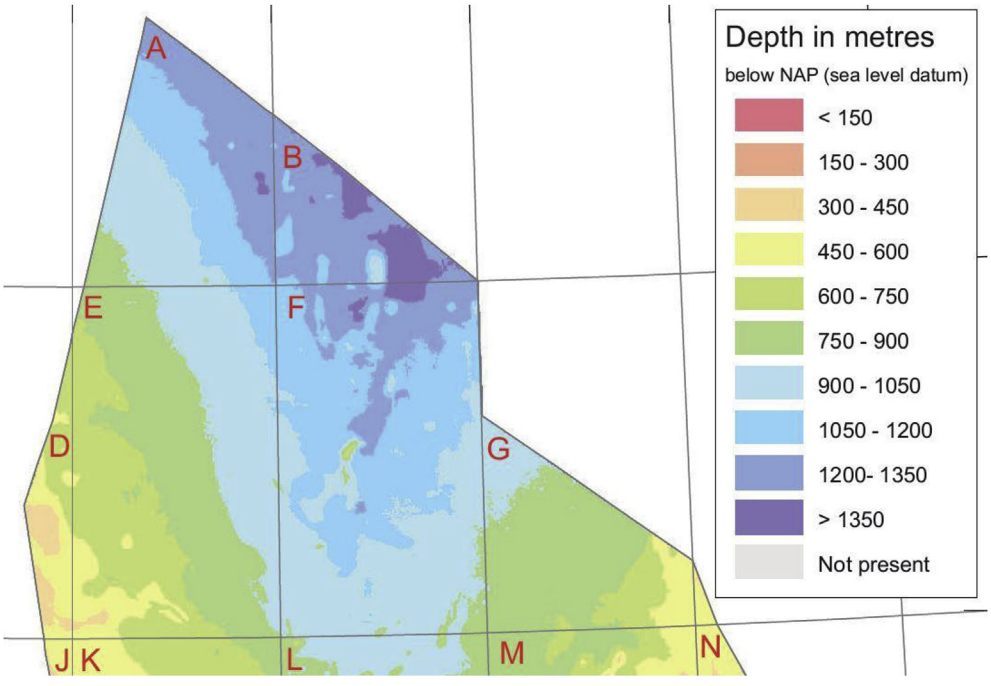

Fig. 4. Depth of the base of the Neogene in the Dutch northern offshore. The base of the Neogene can be considered to be a proxy for the depth of the MMU and base of the SNS delta. The map shows that the base of the delta reaches its greatest depth in the northeastern A blocks, the B blocks and the northernmost F blocks (Modified from Kombrink et al., 2012a).

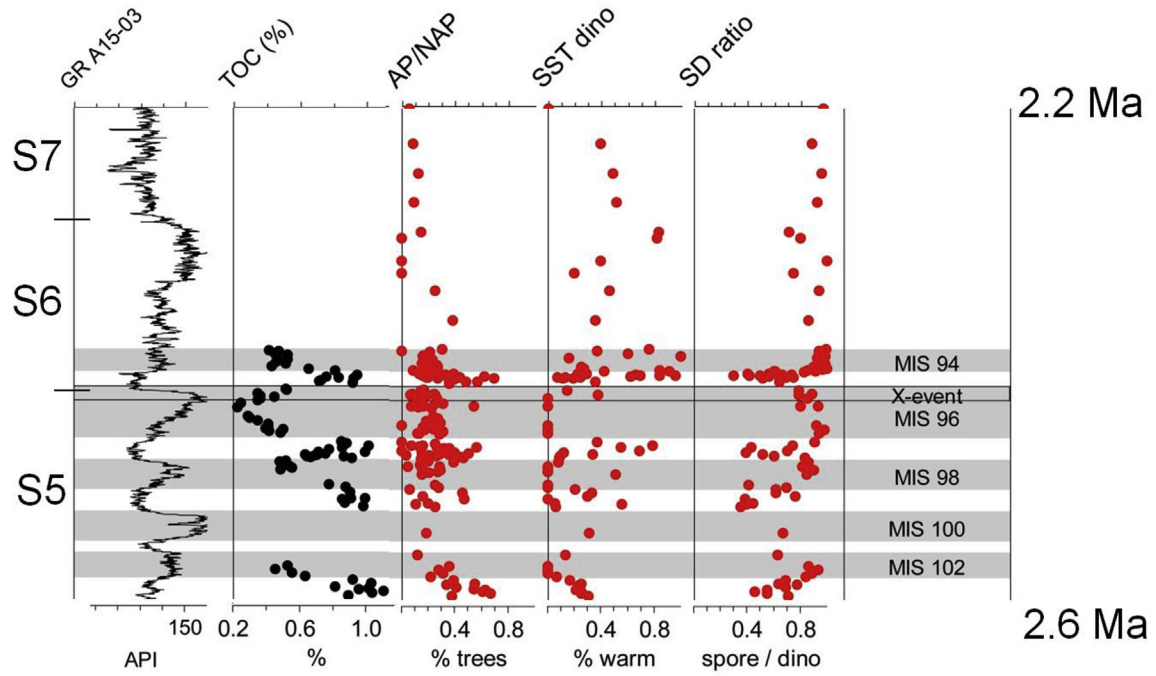

Fig. 5. Sequences S5 to S7 of the Southern North Sea Delta were deposited during an alternation of glacial and interglacial periods. Detailed palynological and geochemical data from well A15-03 (Donders et al., 2018) reveal the climate signal in the delta sediments. The glacial intervals are highlighted in gray and annotated with MIS (Marine oxygen Isotope Stage). Even numbered stages have high $\delta^{18}O$ and correspond to glacial events and uneven MIS have low $\delta^{18}O$ and represent interglacials. GR = gamma ray; TOC = total organic carbon; AP/NAP = ratio of tree to non-tree pollen = tree/herbs (proxy for land surface temperature); SST dino: sea surface temperature based on dinoflagellate cyste; SD ratio = sporomorph to dinocysts ratio, indicative of the relative terrestrial versus marine contribution to organic matter input depending on the sea level.

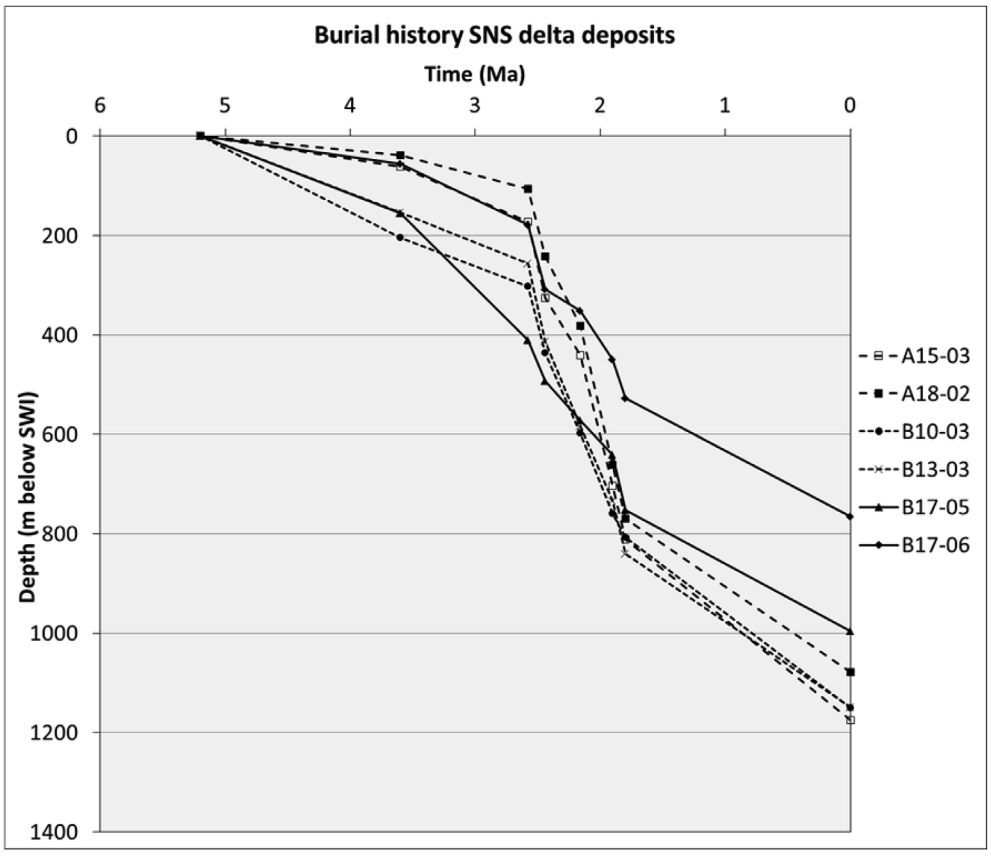

Fig. 6. Compacted burial history of the Southern North Sea Delta deposits at 6 well locations shows that sedimentation rates during deposition of the delta sequences were very high (especially during deposition of S5 -S13 sequences from 2.58 to 1.8 Ma at these well locations). The sedimentation rates continued to be relatively high (> 200 m/Myr) after deposition of the delta deposits until present-day.

entire study area and extended southward into the northern parts of onshore Netherlands (Laban and Van der Meer, 2011; Lee et al., 2012). Laban and Van der Meer (2011) indicate that there is no evidence for a connection of the Scandinavian and British ice sheets in the Dutch part of the North Sea during the Saalian. The Scandinavian ice sheet covered the southeastern part of the Dutch North Sea and northern parts of onshore Netherlands (Laban and Van der Meer, 2011). Possibly the Saalian ice sheet did not reach the study area in the northern offshore. The Late Weichselian – British – ice sheet extended only into the northwestern part of the Dutch North Sea (Hughes et al., 2016; Laban and Van der Meer, 2011). Subglacial tunnel valleys were formed during each of the glaciations, and especially during the Elsterian (Janszen, 2012). Tunnel valleys reach maximum depths of a few hundred meters. During glacial times, outside the areas covered by ice sheets, periglacial conditions induced the formation of regional permafrost. Modelling of the permafrost depths during the Weichselian in onshore Netherlands showed that permafrost could have extended to depths of 120–200 m (Govaerts et al., 2015).

Activation and reactivation and vertical growth of salt tectonic structures during and after deposition of the delta sediments influenced the geometry of the S1-S13 sequences, leading to anticlinal trapping structures and faulting in the delta sediments overlying the salt structures.

Key aspects of the present-day hydrogeologic framework of the SNS delta are related to the geometry of the delta sequences in combination with lithofacies distribution and location of fault and fracture zones. Characteristic features of the geometry of the delta are the sloping surfaces of the delta sequences (clinoforms) with the more steeply dipping delta front sequences occurring basinward of the more gradually dipping delta plain topsets. The lithofacies distribution in the delta shows an overall coarsening of the delta sequences from clays/silts in the predominant prodelta deposits of units S1-S3 to predominant very fine sands of the delta plain deposits of units S12-S13 (Ten Veen et al., 2013). In addition, observed internal layering and associated variations in lithological properties of the clinoforms form a detailed complex of silty/sandy aquifer and clayey/silty aquitard layers. The porosity of the delta sequences is high (> 20% to about 40%).

The current pore fluid pressures in the delta are normal to close to normal in the delta (Fig. 7). This suggests that the competition between pressure generating mechanisms (such as ongoing sedimentary loading, in-situ gas generation), compaction of the SNS delta deposits and pressure dissipating mechanisms (groundwater flow/dewatering of the sediments) are in equilibrium. Paleo pore fluid pressures and groundwater flow in the delta and overlying deposits will have been influenced by loading and unloading of ice sheets (Elsterian ice sheet in particular) and the formation and melting of regional permafrost. The extent of this influence has not been quantified in the study area.

3. Shallow gas in the Southern North Sea Delta

3.1. Distribution of shallow gas

The shallow gas fields (Fig. 1), gas shows encountered during drilling as well as seismic indicators of gas provide insight into the spatial distribution of gas in the SNS delta deposits. Free gas is usually already visible on seismic at low saturations (2-3%). Ten Veen et al. (2013) mapped about 130 bright spots based on seismic amplitude. The distribution of the bright spots, as indicators of gas-filled sand layers, show that there are no bright spots in the sequences S1-S3, that non-stacked foreset type bright spots are exclusively related to sequence S5, elongated bright spots occur throughout the area in sequences S5, S6, S11 and S12, and stacked 4 way dip bright spots dominate in topset beds of the sequences, while bright spots have also been identified in sediments overlying S13 in some locations (Ten Veen et al., 2013). Bright spots dominate in S5 based on the size of the bright spots (as percentage of total bright spot size) and the number of bright spots (as percentage of total number of bright spots). Sequence S12 contains a small number of large bright spots.

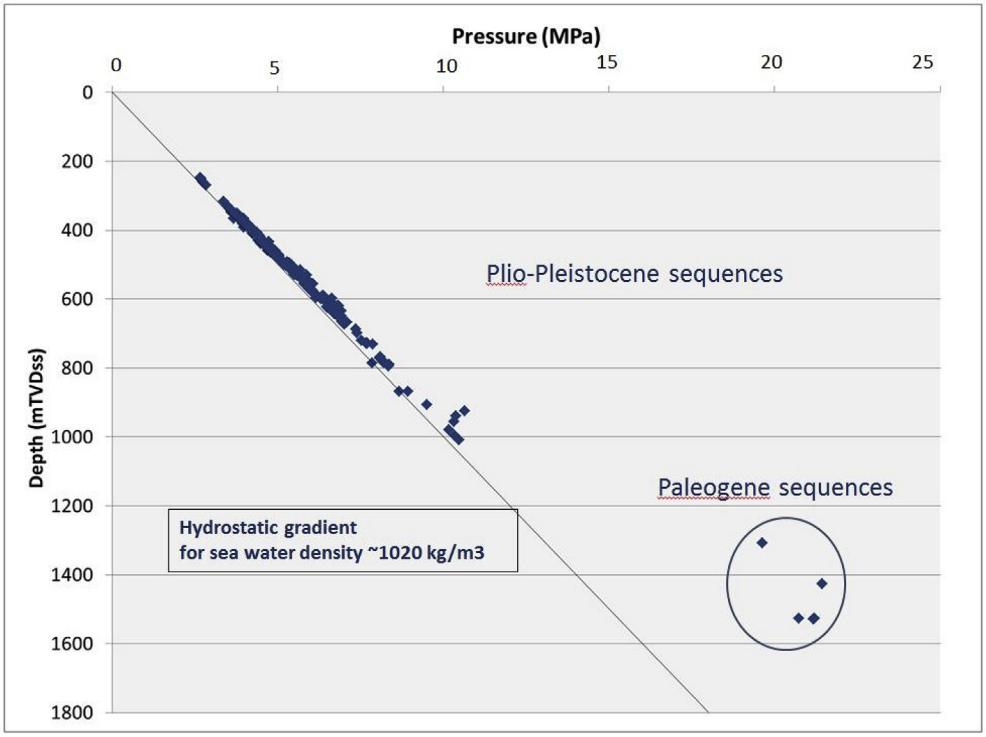

Fig. 7. Cross plot of pore fluid pressure versus depth showing that the pressures in the Plio-Pleistocene Southern North Sea Delta sequences are hydrostatic to close to hydrostatic.

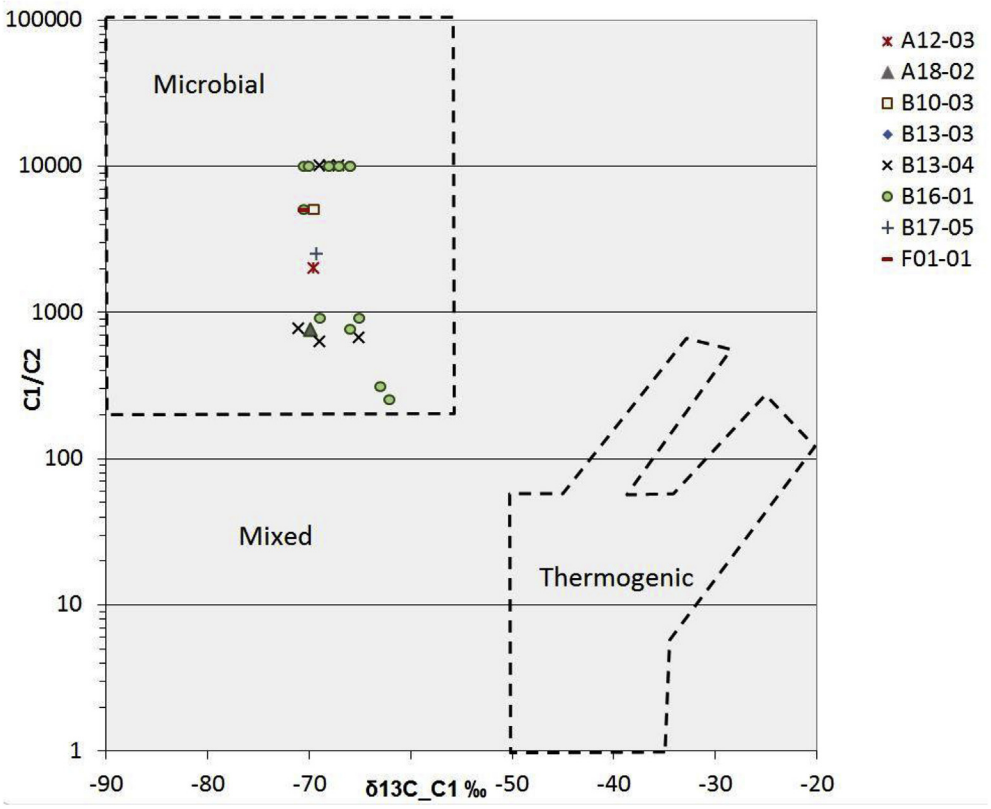

Fig. 8. Bernard cross plot of the methane/ethane ratio (C1/C2) versus $\delta^{13}C/C1$ (Bernard et al., 1978; Whiticar, 1999) of gas samples from the Southern North Sea Delta deposits, showing the microbial signature of the gases. The measured data are from Swint (1999), with the exception of the publicly available data for F01-01 (www.nlog.nl).

3.2. Geochemical composition of shallow gas

There has been a long term debate about the origin of shallow gas in the SNS delta (microbial or thermogenic origin) (Schroot et al., 2005; Ten Veen et al., 2013, 2014). In general, gases of microbial origin are almost exclusively methane, sometimes with small amounts of ethane and propane, i.e. the gas is dry (Katz, 2011). In contrast, thermogenic gas can be dry (such as dry, post-mature thermogenic gas), or can contain significant concentrations of wet gas components (ethane, propane, butanes) and condensate (C5+ hydrocarbons). Stable isotope ratios ($^{13}C/^{12}C$ and D/H; D = deuterium, the heavy isotope of hydrogen) represent, besides compositional data, important parameters for the assessment of the sources and origins of natural gases (Bernard et al., 1976; Schoell, 1983, 1988; Whiticar et al., 1986; Whiticar, 1994, 1999). Methane of microbial origin is more depleted in the heavy isotope of carbon,^{13}C: $\delta^{13}C/C1 < -50$ ‰PDB in comparison with methane of thermogenic origin with $\delta^{13}C/C1$ ranging from roughly −50‰ to −20‰PDB (Whiticar, 1994, 1999).

Measured geochemical compositions of shallow gas from the northern Dutch offshore in the A, B and northernmost F blocks show that the gas encountered in the SNS delta sequences is very dry at wells A12-03, A15-02, A18-02, A18-02-S2, B10-03, B13-03, B13-04, B16-01, B17-05, F01-01 and F02-B-01 (percentage of methane of > 99%). The Bernard-type of cross plot of C1/C2 ratio versus $\delta^{13}C/C1$ (Bernard et al., 1978; Whiticar, 1999, Fig. 8) shows that the measured values $\delta^{13}C/C1$ are between −62‰ and −70.6‰ and in the realm of microbial gas. Hence, the very dry nature of the gas and measured carbon isotopic composition of the methane of gas accumulations in the SNS delta deposits are representative of a microbial origin of the gas.

Such a microbial origin might be a primary or secondary microbial origin. A primary microbial origin involves the microbiological decay of organic matter by methanogenesis, an anaerobic process by methanogens (archaea) that uses substrates, such as bicarbonates and acetate to form methane. Secondary microbial origin includes the biodegradation of oil (Claypool et al., 2001; Head et al., 2003, 2014; Larter et al., 2005; Sweeney, 2001) and - thermogenic - gas (James and Burns, 1984; Larter et al., 2005). Biodegradation of oil and gas may occur during migration and in the reservoir. In-reservoir petroleum biodegradation by methanogenesis is the main process according to Head et al. (2003, 2014).

Observations from mud and gas logs indicate that the amounts of total gas and methane are mostly much larger in the Dutch SNS delta deposits in comparison with those recorded in Cenozoic sequences below the delta deposits (Fig. 9 shows an example), suggesting that in-situ generation - by microbiological decay of thermogenically immature organic matter - plays an important role in charging shallow gas occurrences.

In the following we evaluate first whether the key conditions required for such primary microbial gas generation are fulfilled in the Dutch SNS delta.

4. Microbial gas generation

4.1. Key conditions for primary microbial gas generation

The two basic conditions that need to be fulfilled to enable primary microbiological generation of gas are the presence of organic matter and an active microbial population.

The preservation of organic matter in the sediments after deposition is enhanced by high rates of sedimentation associated with deposition of organic matter (Clayton, 1992; Schneider et al., 2016).

Microbial activity by methanogens requires that the following conditions are fulfilled (e.g. Katz, 2011):

- Anoxic conditions
- Temperatures < 80 °C
  - o Optimal temperatures for microbial activity: 35-45 °C (Katz, 2011); 30-50 °C (Clayton, 2010, oral communication), while microbial activity slows down fast at temperatures exceeding 65 °C
- Presence of sufficient pore water and pore space for a microbial population to grow

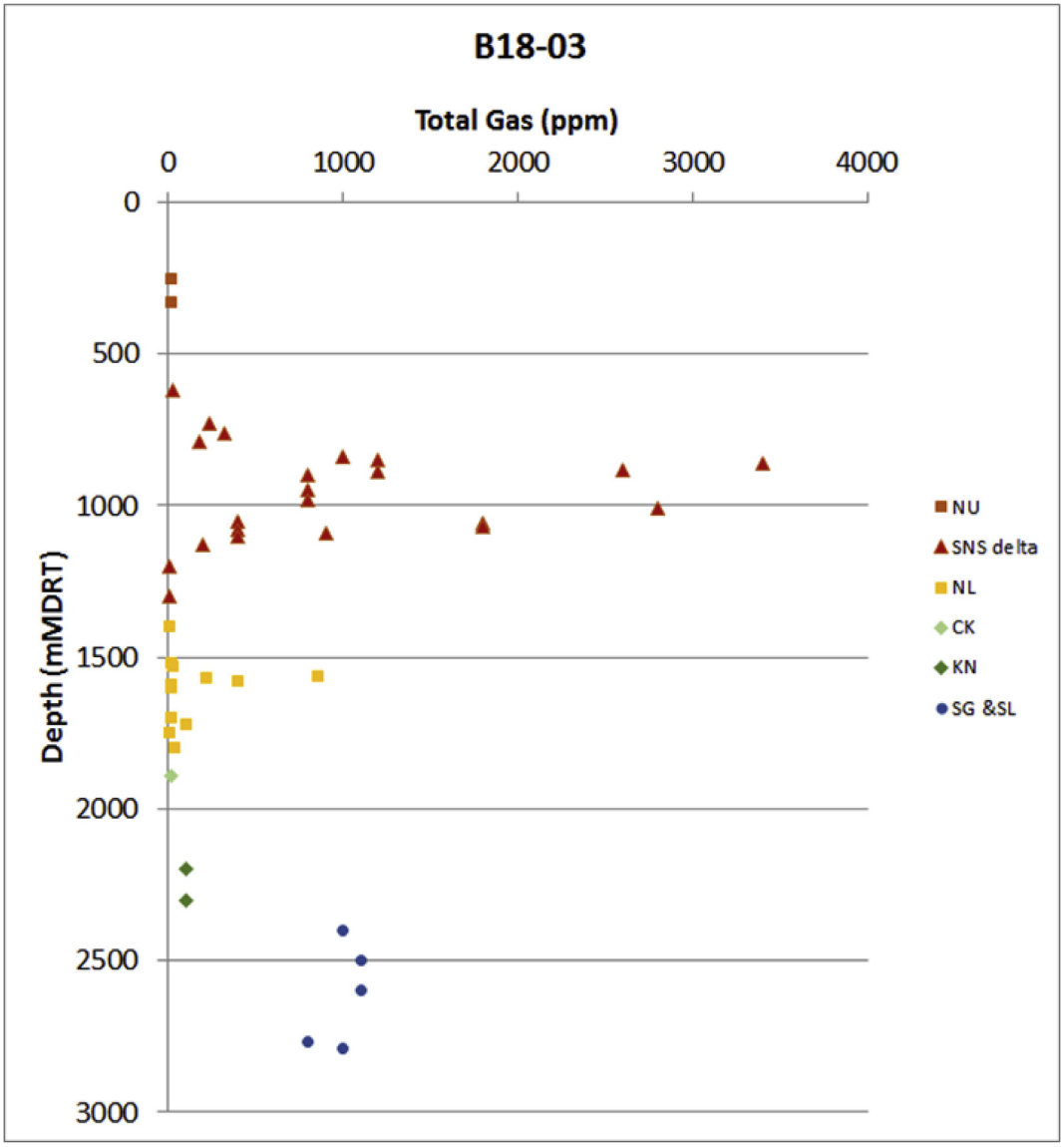

Fig. 9. Cross plot of log derived amounts of total gas versus measured depth at well B18-03 showing elevated values of total gas in the Upper Jurassic-Lower Cretaceous Scruff and Schieland groups (SG & SL), low values of total gas in the overlying sedimentary sequences of Cretaceous age {Rijnland Group (KN) and Chalk Group (CK)} and Paleogene age and greatly increasing amounts of total gas in the sedimentary sequences of the Southern North Sea Delta (gas log data from www.nlog.nl).

- Near absence of sulphate
- Absence of high salinity pore water. Methanogenic activity may slow down or be inhibited by high salinity of the pore water (see also Head et al., 2014).

The overall yield is controlled by the heating rate, i.e. by sedimentation and geotherm during peak microbial activity. Hence, conditions for an optimal yield are low sedimentation rates when the organic matter is in the temperature zone of peak microbial activity.

4.2. Conditions for microbial gas generation in the Southern North Sea Delta

4.2.1. Presence of organic matter

The very high sedimentation rates during deposition of the delta deposits (Fig. 6) are favorable for the preservation of syn-sedimentary organic matter. Lithological logs and geological reports of boreholes report the occurrence of organic matter in the Dutch SNS delta sequences. Fig. 10 shows values of total organic carbon (TOC) measured in a number of wells. The TOC values range from less than 1%–5%, and are mostly between 1% and 2%. The organic matter is mostly land plant matter (Donders et al., 2018; Ten Veen et al., 2013) and is thermogenetically immature at the shallow depths of the delta deposits.

An interesting finding of a detailed study of the variation in %TOC in offshore block A15 showed a clear relation with climate changes and associated sediment types in the delta (Donders et al., 2018; Ten Veen et al., 2013) (Figs. 5 and 11). The delta sequences S5 to S7 were deposited during an alternation of cold glacial and warm interglacial periods. The interglacials are coupled to high sea levels, relatively coarse-grained sediments and relatively high TOC contents, while the glacials are linked to low sea levels, the most fine-grained sediments and relatively low TOC contents. This phase relation has been established independently for an onshore site at Noordwijk (The Netherlands) on the basis of high resolution benthic stable isotope ratios (Noorbergen et al., 2015). This shows that, at least for the S5-S7 sequences, the highest content of organic matter occurs in reservoir-type sequences.

In general, the presence of organic matter reveals the existence of an

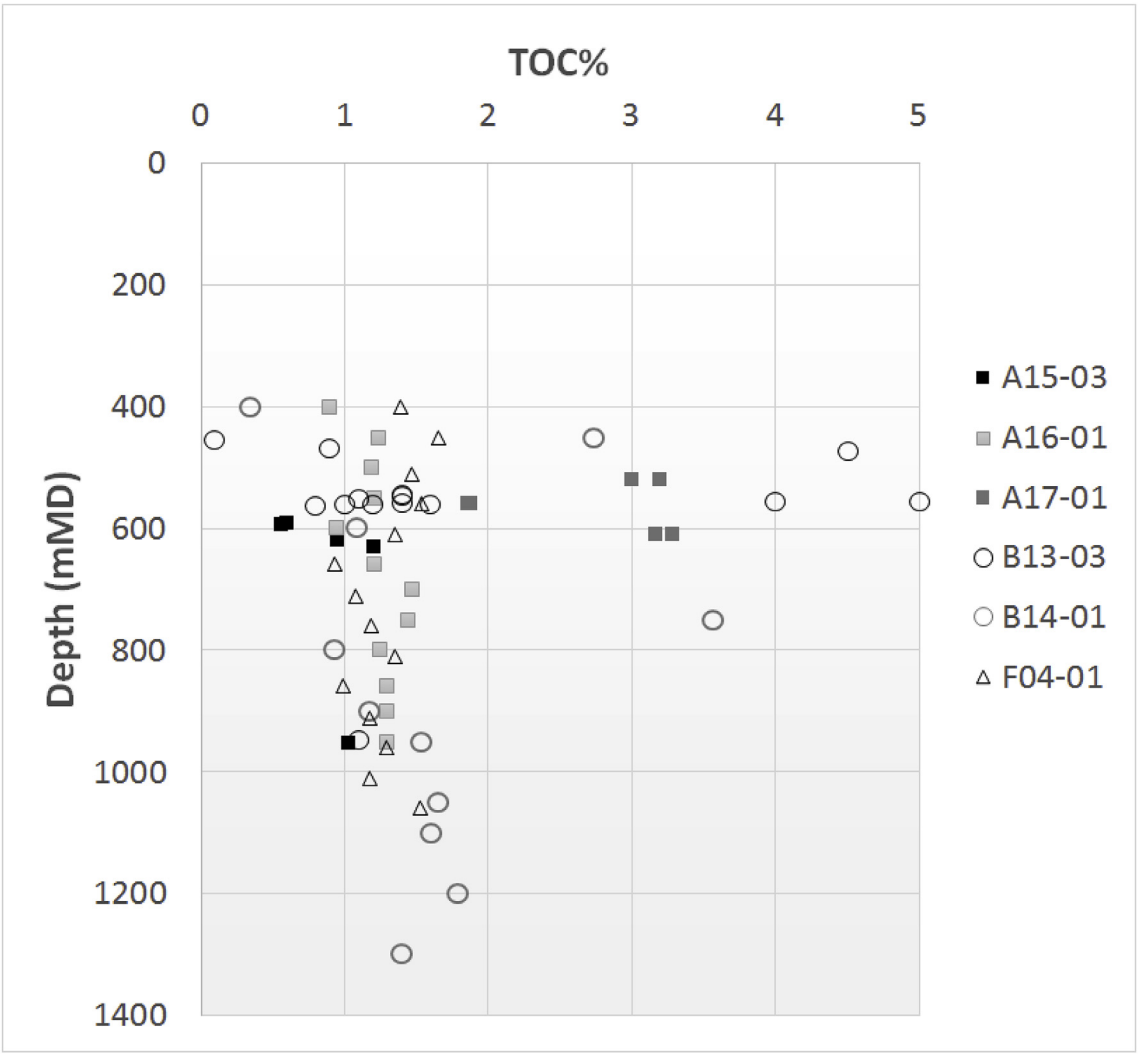

Fig. 10. Measured content of Total Organic Carbon (TOC) in the Southern North Sea Delta deposits at 6 well locations.

intra-delta source for microbial gas generation.

4.2.2. Porosity and salinity of pore water

The SNS delta sequences occur at relatively shallow depths and the porosity of the delta sequences is high (> 20% to about 40%).

There is no publicly available information on geochemical composition or salinity of the pore water. Salinity or total dissolved solids content of pore water can be estimated from measured pressures in the pore water, or gradient of measured pore water pressures within a single reservoir unit, taking into account the in-situ temperature (Underschultz et al., 2002). The pressure data at 7 well locations (A15-02, B13-03, B13-04, B16-01, B17-05, F01-01, F02-03) from the TNO in-house pressure database were used to estimate pore water salinity. The pressure analysis resulted in estimated pore water densities of 1050–1070 kg/m^3 at depths of about 350–800 m. These densities correspond to pore water salinities, expressed as TDS, that are higher than seawater salinity and vary from about 60000 to 100000 mg/l TDS. The increased salinity might have a natural cause, for example, being the result of – previous – contact of upward migrating groundwater with salt structures.

4.2.3. Temperature

The other key condition for enabling microbial generation of gas from organic matter in SNS delta sequences is temperature.

The current average thermal gradient for the subsurface of onshore Netherlands is 31.3 °C/km for a surface temperature of 10 °C, based on corrected temperature measurements from oil and gas wells (90% of the temperature values are between 500 m and 3500 m) (Bonté et al., 2012).

Based on an assumed thermal gradient of 31 °C, a sea surface temperature of 10 °C, and an optimal temperature window for microbial gas generation of 30–50 °C, the current optimal depth for microbial gas generation by methanogenesis would be between about 730 and 1200 m.

The temperature distribution in the subsurface at a certain time during history, assuming steady state conditions, principally depends on the spatial variation in basal heat flow, the distribution of bulk thermal conductivities of the subsurface and the temperatures at the ground surface or sediment water interface. Salt (halite) has a temperature dependent thermal conductivity of 5.4 $Wm^{-1}K^{-1}$ at 20 °C to 3.2 $Wm^{-1}K^{-1}$ at 160 °C (Zoth and Haenel, 1988), which is significantly higher than that of clastic lithologies. As a consequence, salt diapiric structures can significantly disturb heat flow. Focusing of heat flow through salt structures will increase temperatures in the top part of the salt structures and in adjacent lithostratigraphic units. This effect will be most pronounced for the SNS delta sequences located at a short distance above very thick salt diapirs.

Different studies have shown that the thermal gradient in on- and offshore Netherlands is not constant, but varies spatially, both laterally and vertically (Bonté et al., 2012; Tambach et al., 2008; Verweij, 2003;

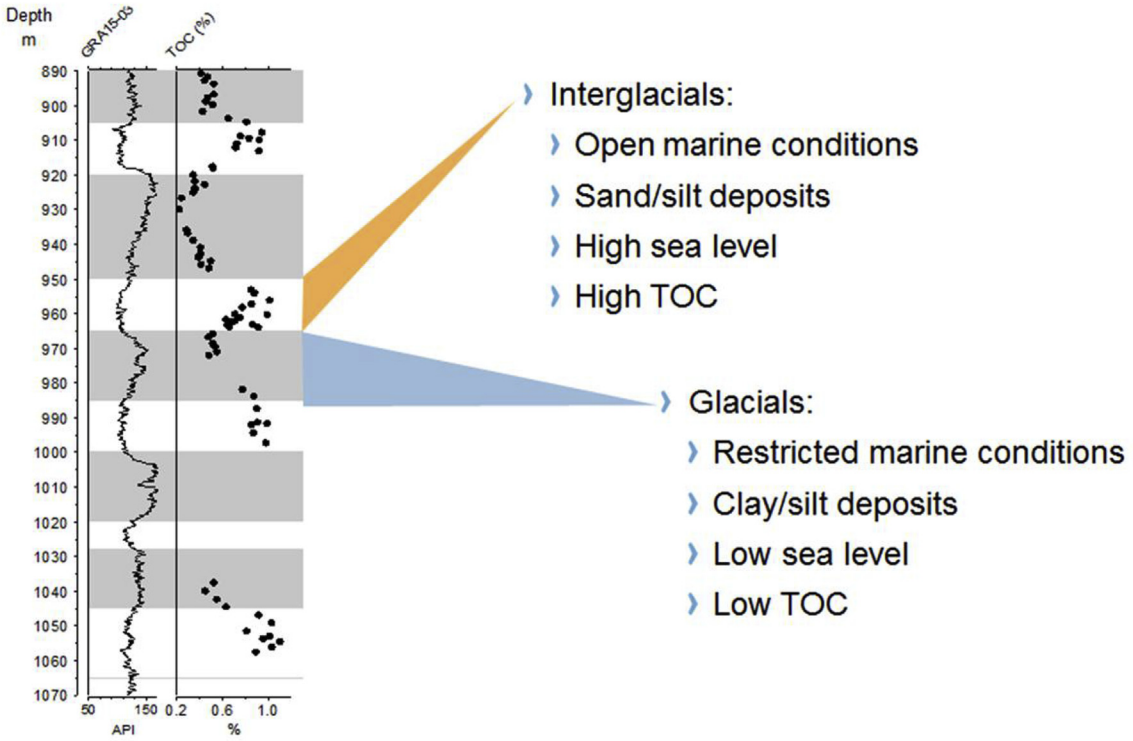

Fig. 11. Variation in TOC content in relation with glacial-interglacial fluctuation. The glacial intervals are highlighted in gray and correspond to MIS 102 to MIS 94 (see also Fig. 5).

Verweij et al., 2005). Fig. 12 presents temperature measurements at 6 well locations in the SNS delta deposits, revealing the existence of different geothermal gradients. This is not surprising since the lithostratigraphic build-up of the subsurface is not layer-cake, and both the lithostratigraphy and the associated bulk thermal conductivities vary spatially over short distances due to differences in lithological composition as well as differences in burial history.

In addition, present-day temperature conditions in the subsurface may not be in equilibrium with current boundary conditions and are in a transient state reflecting in greater or lesser extent paleo surface temperatures. Studies in offshore and onshore Netherlands showed that glacial-interglacial temperature fluctuations affect current subsurface temperatures with magnitudes that decrease with depth (Ter Voorde et al., 2014; Verweij et al., 2013).

The temperature history of the Plio-Pleistocene SNS delta sequences has been influenced by the combined effect of glacial-interglacial surface temperature fluctuations and variations of the burial and porosity history. The variations in burial history are related to variations in sedimentary loading since the start of delta deposition as well as to variations in loading by the advance and retreat of ice sheets. In order to take into account burial history and bulk conductivity variations to assess the temperature conditions in the SNS delta and to study to the

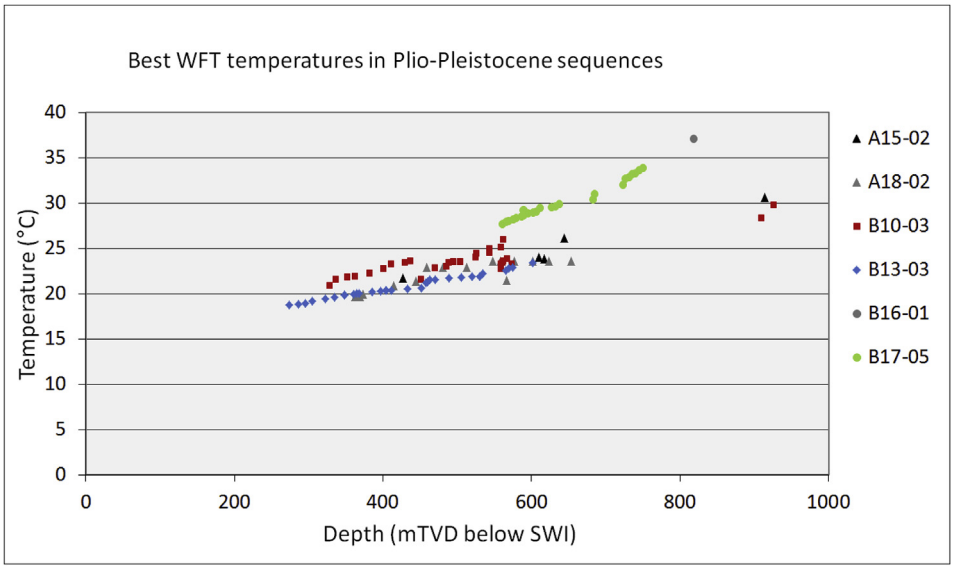

Fig. 12. Cross plots of measured temperatures versus depth beneath sediment water interface (SWI) in the Southern North Sea delta deposits. Selected temperatures were measured during Wireline Formation Tests (WFT).

effect of surface temperature fluctuations on the thermal conditions of the delta sequences, we used detailed 1D basin modelling (PetroMod version 2012 of Schlumberger). Special attention was given to study the effect of surface temperature development over the past 3 Myr. Results of the temperature modelling were used as input for modelling microbial gas generation.

5. Modelling of microbial gas generation history

Paleo and present-day temperatures are one of the implicit results of basin modelling. Basin modelling of the temperature takes important processes and factors into account that influence the present-day temperature condition in the SNS delta sequences, such as its burial and porosity history, bulk thermal conductivity of the sedimentary fill of the Dutch subsurface (as related to lithological composition and porosity), basal heat flow and surface temperature as well as radiogenic heat generation in rocks and transient effects of paleo boundary conditions.

Timing and quantification of microbial gas generation in the SNS delta was studied using a combination of different modelling approaches, and included new detailed basal and surface thermal boundary conditions. 1D modelling was performed at 25 selected well locations covering the distribution area of the Dutch SNS delta (Fig. 1).

The workflow included:

1) 1D basin modelling (using PetroMod of Schlumberger). For most wells we used 1D extractions of existing 3D basin models of the Dutch offshore (covering Carboniferous to recent deposits). In addition, the modelling included new surface temperature data for the last 3 Myr, and detailed chronology (from biostratigraphic data) and detailed lithostratigraphy (from seismic and log interpretation) for the S1 to S13 sequences of the SNS delta. The basin modelling reconstructed the evolution from Carboniferous to present-day (Guaipo Sarmiento, 2013). The 1D basin modelling was used to:
   a) Evaluate the impact of rapid surface temperature fluctuations during the last 1 Myr on magnitude of subsurface temperature fluctuations at different depths and on temperature fluctuations in the different delta sequences;
   b) Assess the current optimal temperature depth window for microbial gas generation (assuming 30-50 °C is the optimum temperature window);
   c) Provide input data for 1D modelling of microbial gas generation in the delta sequences, such as current temperatures and paleo geothermal gradient, sedimentation rate, lithology, sediment water interface temperature;
2) 1D modelling of microbial gas generation in the SNS delta deposits (using Biogenix version 4.01; www.c-clayton.com).

Basin modelling was executed, using the following boundary conditions:

Surface temperature. Two boundary conditions were used: 1) a mean surface temperature, estimated by a default function in the basin modelling tool PetroMod, that calculates the evolution of ocean surface temperatures through time, depending on the latitude of the area; 2) surface temperature boundary condition, including a more detailed temperature history for the last 3 Myr based on Bintanja and Van de Wal (2008) (Fig. 13).

Water depth. The same history of water depth was used as applied in existing 3D basin modelling of the Dutch offshore (e.g. Abdul Fattah et al., 2012).

Basal heat flow. After calibration, the final basal heat flow used at the different well locations varied between about 50 and 70 mW/m^2 (Guaipo Sarmiento, 2013) (the highest heat flows were related to well locations, where thick Zechstein salt structures are present, e.g. at B13-02). Measured present-day temperatures were the main data used for calibration at all wells. These temperature data included temperatures measured during drill stem tests (DST), bottom hole temperatures (BHT), extrapolated bottom hole temperatures (BHTX), temperatures measured along hole (AHT) and during wireline formation tests (WFT). Fig. 14 presents examples of the simulated and measured temperatures at 4 well locations showing the relatively high temperatures at B13-02.

5.1. Impact of glacial-interglacial temperature fluctuations on temperature history

Basin modelling of the temperature evolution of the SNS delta deposits aimed to evaluate where, at what location and depths, and when the optimal temperature window for microbial gas generation (30–50 °C) occurred in the SNS delta deposits during its burial history, and to what extent this temperature evolution was influenced by the glacial-interglacial temperature fluctuations.

Fig. 15 compares the simulation results for the subsurface temperature evolution at the top (sequence S13), middle part (sequence S6) and base (sequence S1) of the SNS delta at well location A15-03 for the two different surface temperature boundary conditions during the last 1 Myr. The simulated temperatures indicate that the adjusted more detailed surface temperature boundary condition results in lower subsurface temperatures during the last 1 Myr, including today. The simulation results further show that the surface temperature variations are reflected in the subsurface temperature evolution with decreasing amplitudes of the temperature with depth. Temperature fluctuations are still apparent, but with greatly reduced amplitudes at depths corresponding to the optimal temperature window for microbial gas generation (starting at 30 °C). Fig. 16 shows the simulated temperature history from Pliocene to present-day at wells A15-03 and B13-02. A temperature of 30 °C is reached in the S1-S5 sequences in the Early Pleistocene Calabrian (Calabrian period extends from 1.8 Ma to 0.78 Ma) and in sequence S6 at about 0.5 Ma. Hence, at present-day, sequences S1 to S6 at A15-03 and B13-02 are in the optimal temperature window for microbial gas generation at both locations.

The results of the simulations at all 25 wells showed that: 1) burial history in combination with the average surface temperature evolution has a much greater influence on the temperature history in the delta sequences than the impact of the glacial-interglacial temperature fluctuations, especially after the sequences enter the optimal temperature window (see e.g. Fig. 16); 2) sequences S1 to S5 are in the optimal temperature window for microbial gas generation today; 4) the overall heating rate of the units are low during the last 1.5 Myr, when the sequences are in the optimal temperature window.

5.2. Microbial gas generation

The Hybrid model of Biogenix for microbial gas generation includes first order reaction kinetics to model substrate generation by thermal breakdown of proto-kerogen and the conversion of substrate to methane by methanogenesis at a temperature dependent rate. In the Thermal model of Biogenix the gas generation is calculated by a zero order reaction in which generation is controlled only by the temperature sensitivity of the methanogens.

The microbial generation of gas in the SNS delta was modelled using the Hybrid model of Biogenix version 4.01. We used the standard kinetics for kerogen breakdown available in the Hybrid model of Biogenix, that is based on the kinetic model published by Lorant et al. (2008). For comparison reasons we also show an example of the simulation results of the application of the Thermal model included in the Biogenix software.

Input for Biogenix includes: basic input, such as current water depth, bottom water temperature, maximum depth to be modelled; and burial history, temperature profile, pressure condition (hydrostatic or overpressured), lithology per layer, type of organic matter and TOC content. As described above, the input with respect to burial history and temperature profile was derived from the 1D basin modelling. The Biogenix modelling was executed for a maximum depth of 1500 m, the

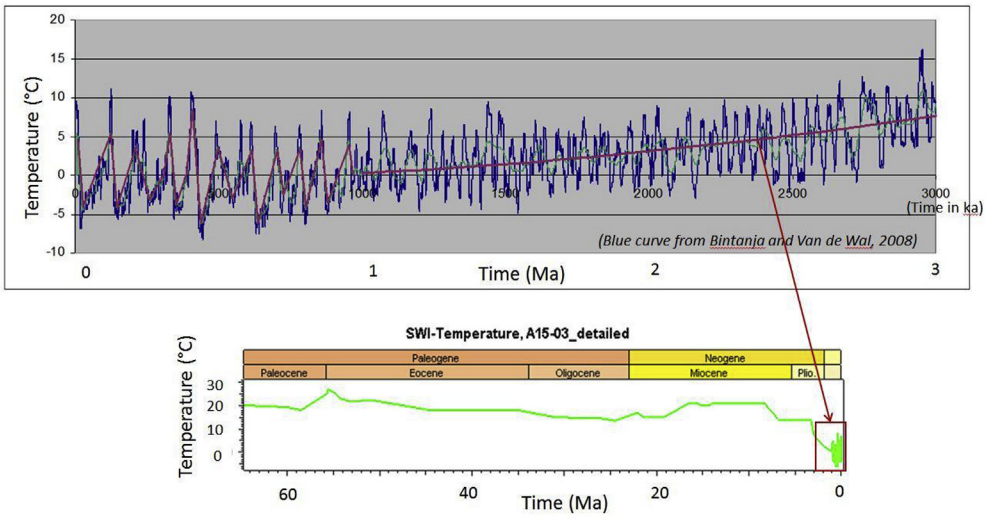

Fig. 13. Surface temperature boundary condition for basin modelling. The detailed boundary condition for the last 3 Myr is based on data from Bintanja and Van de Wal (2008) (Figure at the top); the dark blue curves show the data of Bintanja and Van de Wal (2008) and the red curve represents the derived temperature curve incorporated in the surface temperature boundary condition. (For interpretation of the references to colour in this figure legend, the reader is referred to the Web version of this article.)

sediment package was divided into layers of 20 m thickness with assigned ages, lithologies and temperatures, and hydrostatic pressures. It was assumed that only the SNS delta deposits contain organic matter, that the organic matter is of kerogen type III, TOC content is 1% in all layers of the SNS delta, and that there is no expulsion of gas from the pores. The model output includes, amongst other things, gas generation rate (m^3STP/m^3 rock/Myr); total volume of gas generated (m^3STP/m^3 rock) and part of the generated gas volumes that is adsorbed, in solution in the pore water and occurring as free gas in the pores. The free gas is also indicated as gas saturation, i.e. the percentage of porosity occupied by free gas. Fig. 17a–e shows the results for a selection of well locations. The simulation results indicate that for the assumed conditions, the SNS delta deposits generate microbial gas at present-day. The generation already starts at shallow depths at the top of the delta deposits where the generated gas is initially adsorbed, at about 600 m depth the generated gas starts to be dissolved in the pore water, and at greater depth it is released as free gas in the pores.

The effect of simulating the microbial gas generation with the Thermal model instead of using the Hybrid model is illustrated in Fig. 18. In general, the gas generation rate is higher for the thermal model and starts already at shallower depths.

The measured values of TOC indicated that most values vary between 1% and 2% TOC (Fig. 10). Fig. 19 shows the simulation results for an assumed constant content of 2% TOC in the delta sequences at well B13-02, using the Hybrid model and maintaining the other standard model input. Doubling of the TOC content causes a doubling of the maximum gas generation rate and doubling of the maximum generated gas volumes. In reality, the TOC content of the delta deposits is not constant throughout the delta: it varies both vertically and laterally. The measured values at B13-03, B14-01 and A17-01 (Fig. 10) show values exceeding 3% TOC in the upper part of the delta deposits. Fig. 20 presents the simulation results of incorporating higher TOC contents at certain depths at well location B13-02: TOC = 4.5% at 480 m, 1.4% at 540 m, 5% at 560 m, 1.6% at 580 m and 1.1% at 940 m. Gas saturations reach values of ≥2% at shallow depths corresponding to the depths of 460 m and 560 m with assigned high TOC values of 4.5 and 5%, respectively.

The different modelling scenarios (scenario using the Thermal model instead of the Hybrid model; scenario for a constant higher TOC content of 2%; and a scenario with locally higher TOC contents) all indicate that the results of modelling microbial gas generation using the Hybrid model of Biogenix for the initial standard conditions can be considered to provide relatively conservative estimates of the microbial gas generation potential of the SNS delta deposits. It is interesting to note that the conservative estimates of microbial gas generation show gas saturations of ≥2% already at shallow depth in the northeastern part of the Dutch SNS delta in comparison with other parts of the delta (e.g. for well location B13-02 at about 600 m depth, for F04-01 at about 1000 m depth). As stated above, such low gas saturations might already be visible on seismic.

In order to provide an indication of microbial gas volumes generated in the Dutch SNS delta as a whole, we estimated volumes based on the simulation results, using the approach given in Clayton (1992). Taking the simulated methane volume generated of ~5 m^3STP/m^3 source rock with 1%TOC (Fig. 17) (corresponding to a volume of $5*10^6$ m^3 STP/km^2 for source rock of thickness of 1 m), and a distribution area of the Dutch SNS delta deposits where gas is generated of about 30000 km^2 results in: $15*10^{10}$ m^3STP ~150 bcm of microbial gas generated in the delta per 1 m thickness of source rock (TOC 1%). It seems that the delta has been able to generate more than enough microbial gas to fill the estimated volumes of shallow gas prospects of 36–118 bcm GIIP given by Van den Boogaard et al. (2013). Hence, generation of microbial gas is not the limiting factor for forming shallow gas accumulations in the delta deposits. Key factors that determine whether a gas accumulation occurs at present-day are focused migration, entrapment and preservation of the accumulated trapped gas.

6. Migration, entrapment and leakage of microbial gas

The shallow gas accumulations existing today in the SNS delta sequences have resulted from migration and entrapment and remigration since the beginning of microbial gas generation, i.e. since about Early Pleistocene Calabrian times (Fig. 16).

Gas generation, migration, entrapment and leakage during Early Pleistocene to recent times developed under highly dynamic pressure, stress and temperature conditions that resulted from the combined effect of sedimentary loading (Fig. 6), advance and retreat of ice sheets, sea level changes and glacial-interglacial temperature fluctuations (Fig. 13). The current presence of gas in intra-delta reservoirs is the final result of gas charging and leakage of the traps in the Plio-Pleistocene delta under these highly dynamic conditions.

6.1. Migration and Carrier/reservoir beds

Migration and entrapment of microbial gas generated in the SNS delta at present-day take place under normal to close-to-normal pore pressure conditions (Fig. 7). The migration under such present-day circumstances involves movement of methane dissolved in groundwater and buoyancy-driven separate phase movement of free gas towards

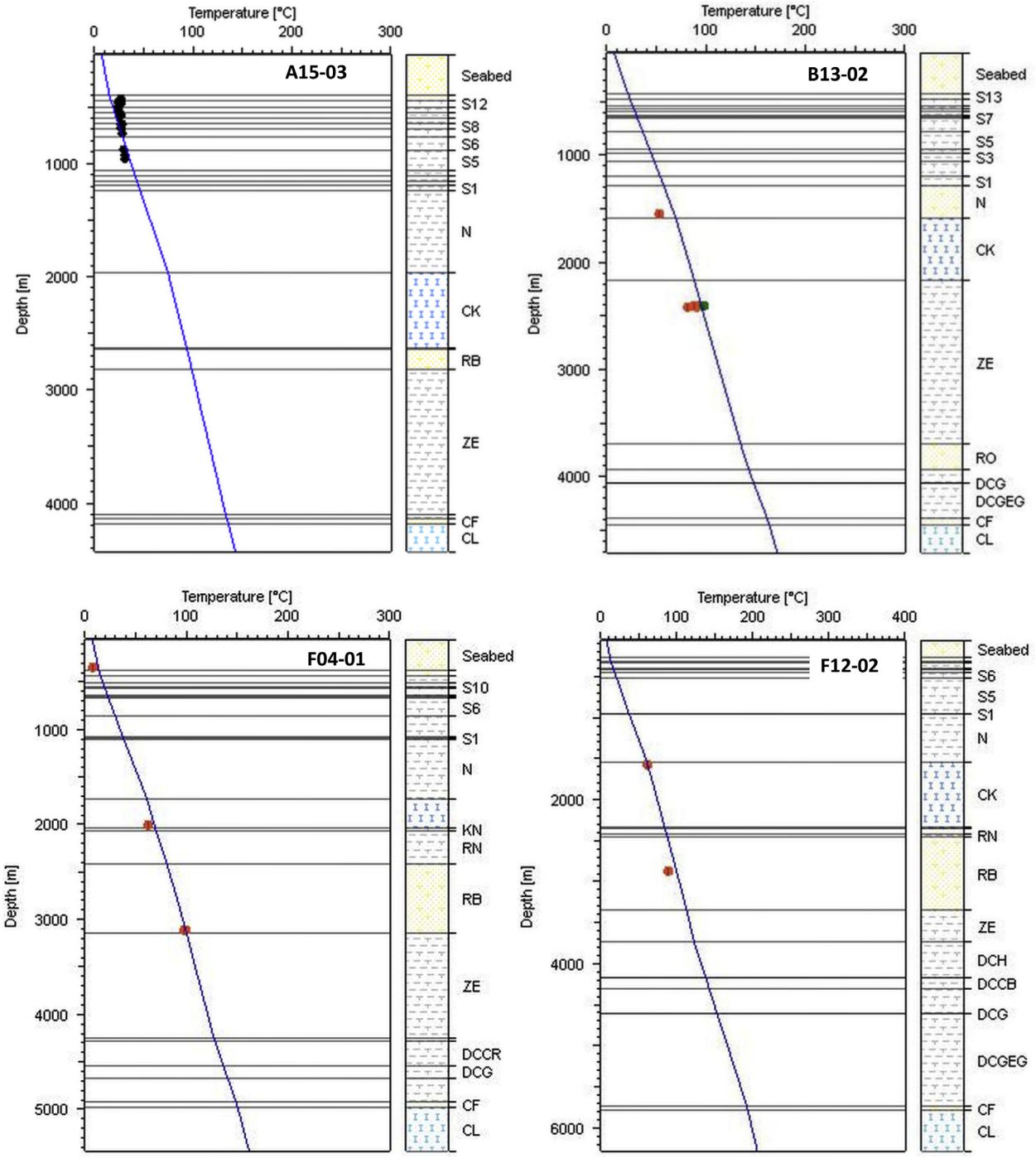

Fig. 14. Cross plots of simulated and measured present-day temperatures versus depth at A15-03, B13-02, F04-01 and F12-02 (From Guaipo Sarmiento, 2013). Measured temperatures include DST and BHTX (green dots), BHT (red dots) and AHT and WFT (black dots). The simulated temperature at 1000 m depth is 37 °C at A15-03, 46.6 °C at B13-02, 36.1 °C at F04-01 and 39.2 °C at F12-02. (For interpretation of the references to colour in this figure legend, the reader is referred to the Web version of this article.)

conventional stratigraphic and structural traps. The ongoing dewatering of the sediments by sedimentary loading will have a vertical component of groundwater flow. Because of decreasing pressures along the flow path, methane in the water will be exsolved and introduced as free gas in the pores at shallower depths.

The amount of organic matter in the SNS delta deposits varies, being higher in the coarser-grained sediments deposited in interglacial times in comparison with the over- and underlying finer-grained sediments deposited in glacial times (Fig. 11). The interglacial sediments may thus act both as principal source rock and as carrier bed and/or reservoir for microbial gas. Measurements of – helium - porosity and horizontal permeability on samples taken from carrier/reservoir beds at 7 wells (A12-03, A15-03, A18-02-S2, B10-03, B13-03, B17-05, B17-06) show that the porosity varies between 24% and 44%, and the horizontal permeability between 2.5E-16 m^2 (0.25 mD) and 4.5E-12 m^2 (4600 mD) at depths of 470–700 mMD (based on data derived from www.nlog.nl).

The direction of buoyancy-driven migration through the carrier rocks will be updip towards stratigraphic and structural traps. Given the geometry of the delta sequences (Fig. 3) the regional updip migration will be directed towards the east. Decreasing pore pressures and

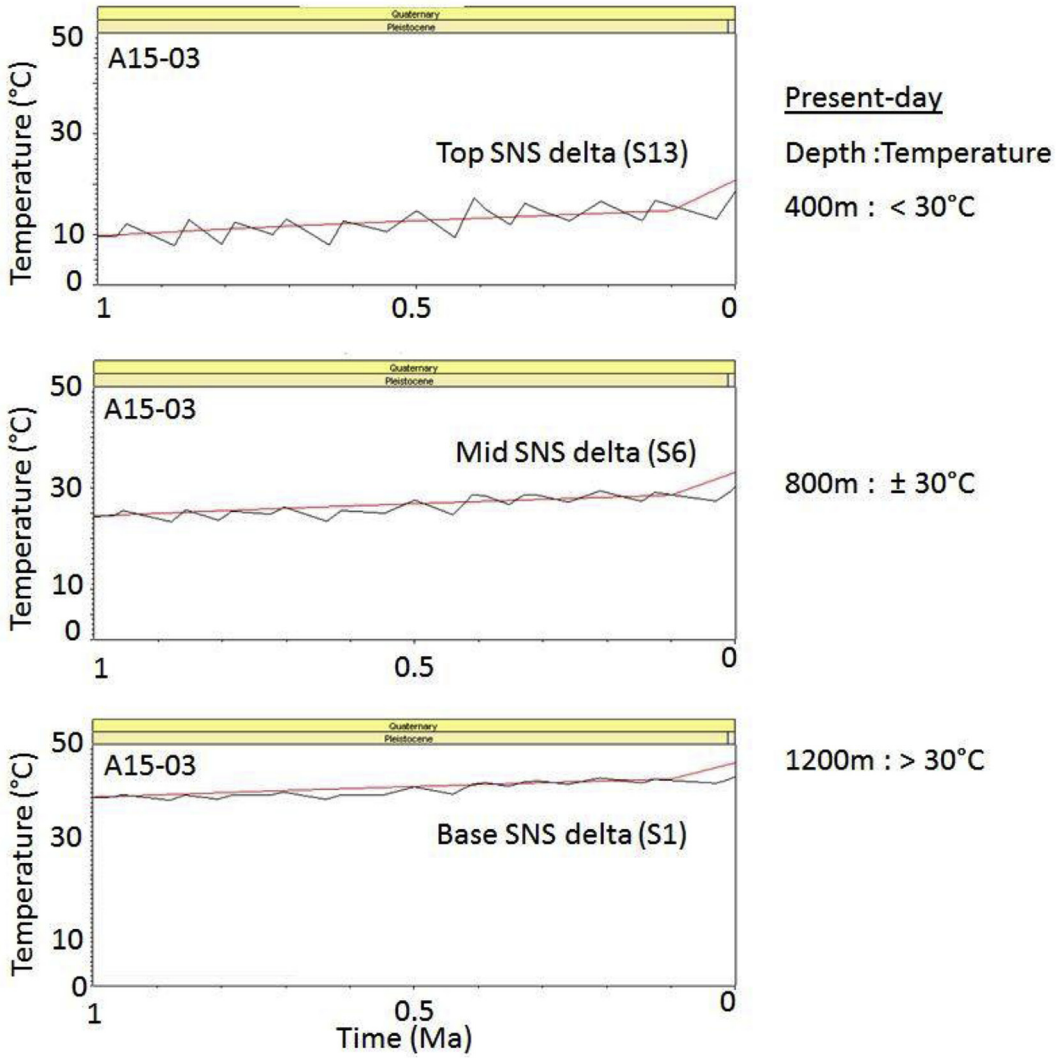

Fig. 15. Simulated impact of glacial-interglacial surface temperature fluctuations on the temperature history (black lines) in sequences S13, S6 and S1 at well A15-03 in the Southern North Sea delta from 1 Ma to present-day. At present-day the temperature at the top of the SNS delta is < 30 °C; in sequence S6 the temperature is about 30 °C; and at the base of the delta the temperature is > 30 °C. The red lines show the impact of the mean surface temperature, estimated using a default function in the basin modelling tool PetroMod. (For interpretation of the references to colour in this figure legend, the reader is referred to the Web version of this article.)

associated decrease of the density of the migrating gas during updip migration, especially in the more steeply dipping delta front sequences, will increase its buoyancy along the migration path. Upon reaching the flatter topsets of the delta, the updip component of the buoyancy driving force decreases. Such focusing of gas migration through the foresets towards the topsets of the delta sequences is supported by the finding that gas saturations in the stacked 4way dip bright spots and in drilled stacked bright spots in particular, have higher gas saturation than the other type of bright spots (Ten Veen et al., 2013). The properties of the clayey/silty seals of the encountered stratigraphic and structural traps along the migration path will determine whether or not a shallow gas will accumulate or leak through the seal.

6.2. Entrapment and seals

The seal capacity of the intra-delta sealing layers for hydrocarbons is given by the height of the hydrocarbon column that the layers hold prior to leaking. For a water-wet sealing layer this is strongly controlled by the capillary entry pressure of the seal which in turn is a function of the pore-throat size distribution along the largest interconnected pore throat path through the seal. The capillary seal capacity of a layer is not influenced by the thickness of the seal, because capillary forces at the interface between reservoir and seal are not related to the thickness of the seal. A water-wet seal will act as a capillary seal for hydrocarbons until the buoyancy pressure of the hydrocarbon column exceeds the capillary entry pressure of the seal (Ingram et al., 1997; Sylta, 2005). If the buoyancy pressure exceeds the capillary entry pressure the hydrocarbons will leak through the seal by two-phase Darcy flow. Hydrocarbon saturations required to breach mudstone seals are highly variable, ranging from < 1% to > 20% (Kurtev et al., 2012). Following Darcy's law, the leakage rate is directly related to the buoyancy pressure of the hydrocarbon column, the relative permeability of the seal and inversely related to the thickness of the seal. The leakage rate through a thin seal will be much faster than that through a thick seal for the same (relative) permeability. Below thick seals and during continued charging of the trap, the hydrocarbon column height continues to increase after capillary seal breaching, if the leakage flux is smaller than the flux into the trap. Under such dynamic conditions the hydrocarbon column height that can be maintained by the top seal will be greater than the maximum height of the hydrocarbon column related to the capillary seal capacity. After charging of the trap has stopped, leakage through the top seal will continue by two phase Darcy flow, and the

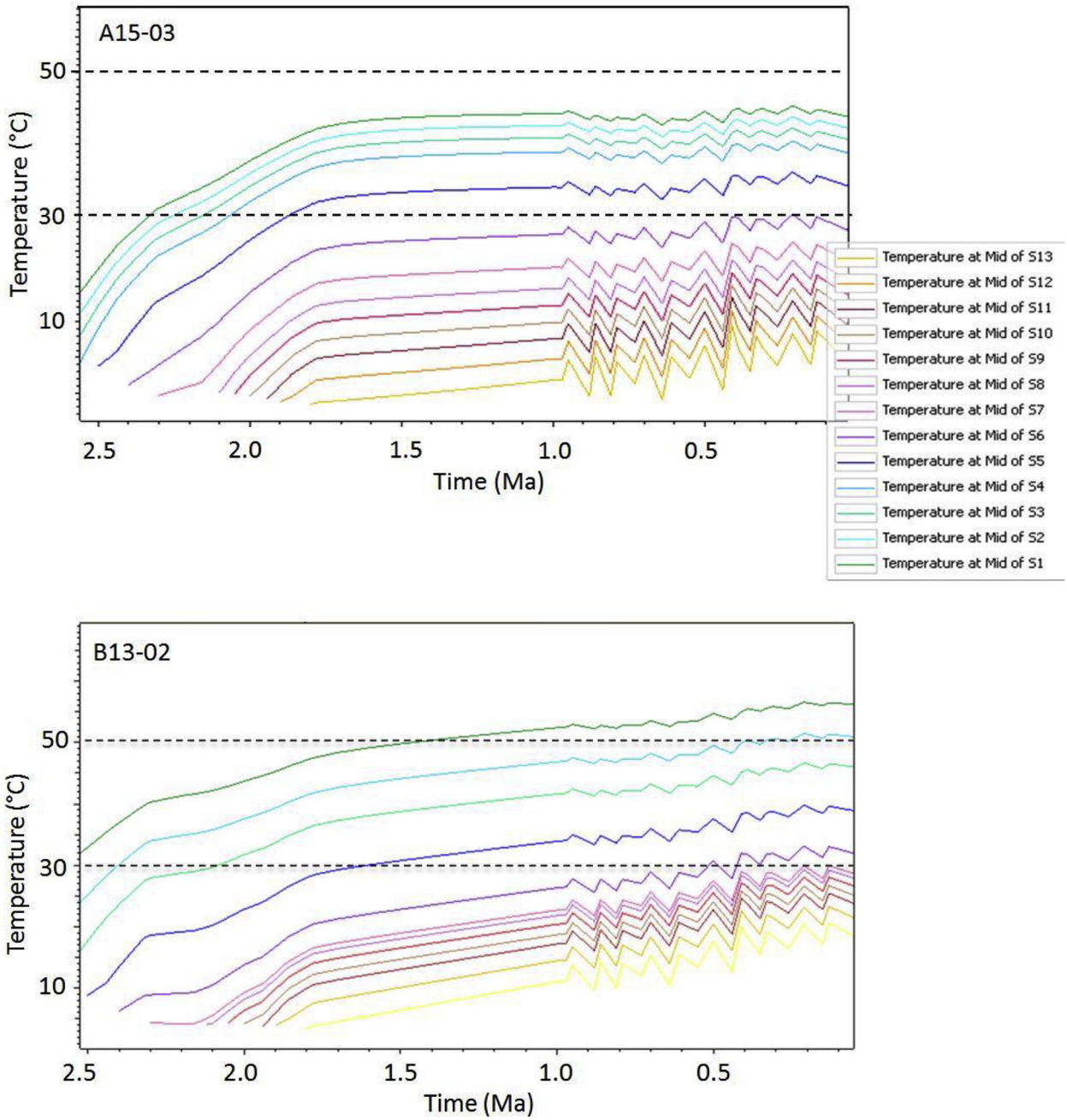

Fig. 16. Simulated impact of glacial-interglacial surface temperature fluctuations on the temperature history in the different sequences of the Southern North Sea Delta at wells A15-03 and B13-02 (Modified from Guaipo Sarmiento, 2013). The dashed lines are the boundaries of the optimal temperature window for microbial gas generation (30°C-50 °C).

hydrocarbon column height may decrease again, i.e. the trap may be emptied by leakage through the caprock to a greater or lesser extent in time.

Hence, capillary entry pressures are probably not the only control on maximum column heights of intra-delta mudstone top seals. Charging and top seal leakage history also control maximum and present-day column heights.

Because of lack of public information on the seal capacity of the intra-SNS delta mudstone seals, we developed, tested and applied a systematic approach to evaluate porosity and permeability and capillary seal capacity of mudstones based on new grain-size analysis data and publicly available pressure data (Daza Cajigal, 2012; Ten Veen et al., 2013; Verweij et al., 2014). After testing different approaches we finally selected equations including clay content as important parameter. These equations were developed by Yang and Aplin (2004, 2010) for calculating mudstone porosity and permeability, respectively. The pore throats are calculated from approaches that use the calculated porosities and median grain size, based on equations published by Nakayama and Sato (2002). Knowing the pore throats, the sealing capacity could be determined by estimating the water densities from WFT pressure measurements, and gas densities and gas-water interfacial tensions from established relations using known temperature and pressure changes with depth (NIST Chemistry WebBook: http://webbook.nist.gov/chemistry/fluid/; Nordgård Bolås et al., 2005, respectively).

The selection of appropriate sealing layers for sampling was based on the evaluation of a combination of logs and hydrocarbon indicators from seismic (bright spots) to identify gas occurrences at 10 wells. The

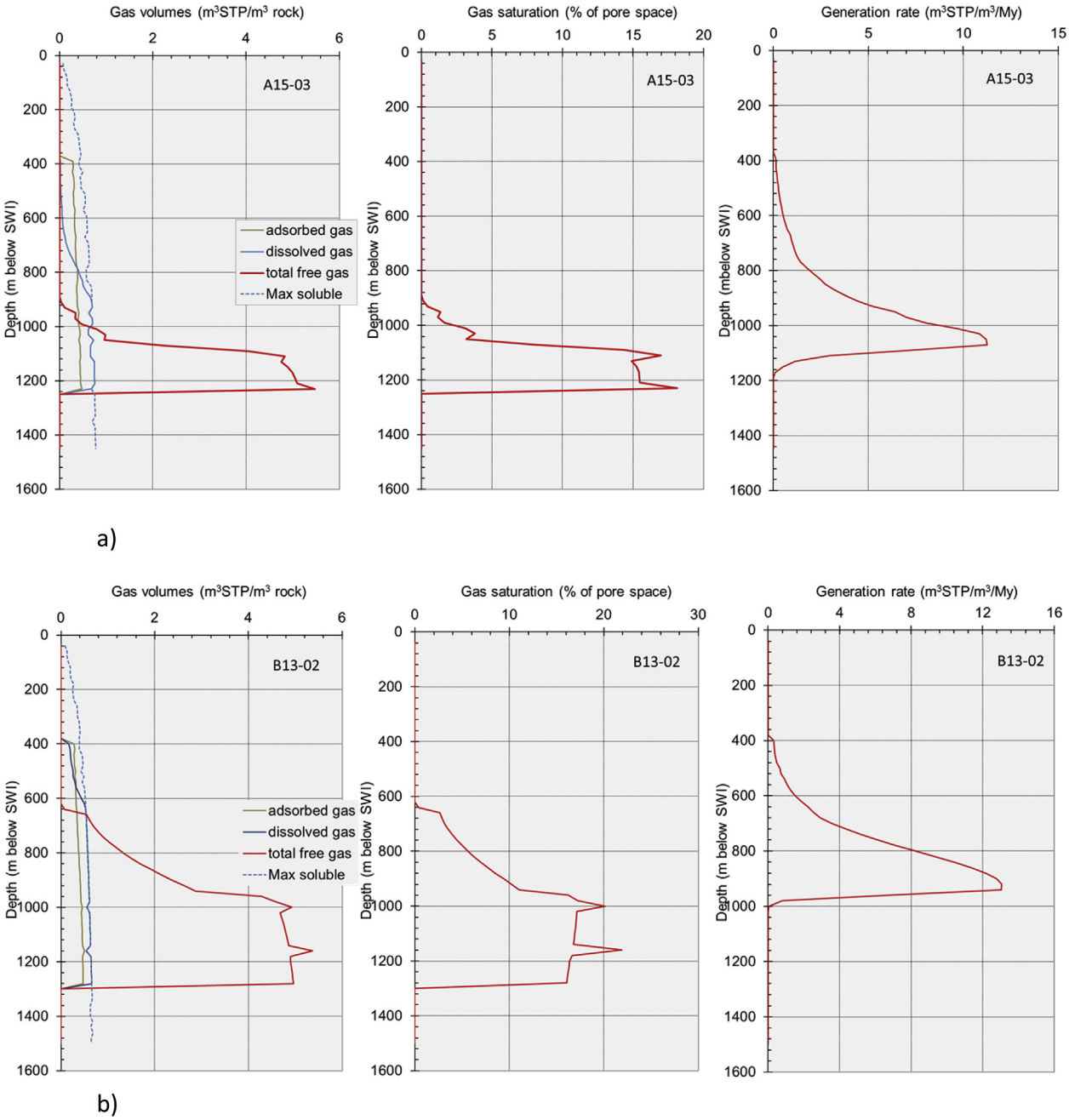

Fig. 17. Results of the simulation of microbial gas volumes, saturation and generation rate using the Hybrid model of Biogenix for TOC = 1% and otherwise standard conditions at the following well locations: a) A15-03, b) B13-02, c) B18-03, d) F04-01, and e) F12-02.

logs included mud logs (providing information on gas peaks), and neutron (NPHI) and density logs (RHOB). The cross-over of NPHI and RHOB log curves are indicative of the presence of gas. Based on the identified gas occurrences and the gamma-ray logs, 45 apparent sealing layers overlying the gas occurrences were selected for sampling (Daza Cajigal, 2012). In total 77 samples (73 cutting and 4 core samples) from these 45 sealing layers in 10 wells (A12-03, A15-04, A18-02, B10-03, B13-03, B13-04, B17-05, B17-06, F01-01, F02-06) were analyzed for grain-size distribution using laser diffraction measurements. The grain size analysis showed that most of the samples are composed of silty clay and clayey silt and are classified as mudstones. Six samples have a sand content of > 20% and classify as sand-silt-clay.

From the grain-size distribution of the sealing layers, a database was constructed with relevant properties such as clay content, median grain size, porosity, permeability and critical pore throat radius. The calculated vertical permeability of the samples of the sealing layers varies between 2.8E-20 m^2 (2.8E-5 mD) and 1.1E-18 m^2 (1.1E-3 mD) and most of the pore throat radii are between 0.5 μm and 1.5 μm. The data base was used to calculate the capillary seal capacity of each layer, which was compared with the gas column calculated using the WFT pressure measurements available for the reservoir underlying the seal and with other indicators of gas column heights, such as the heights of gas occurrences detected from cross-overs of neutron (NPHI) and density (RHOB) logs and information on gas-water-contacts (GWC) from end-of-well reports (Ten Veen et al., 2013).

The calculated capillary seal capacities of the samples vary between approximately 10 and 24 m (Fig. 21). The outliers from the general trend of pore throat radius and capillary seal capacity on Fig. 21 are from samples with a sand content of > 20% (see for example the pore throat radius of 2.4 μm and associated capillary seal capacity of 5.7 m

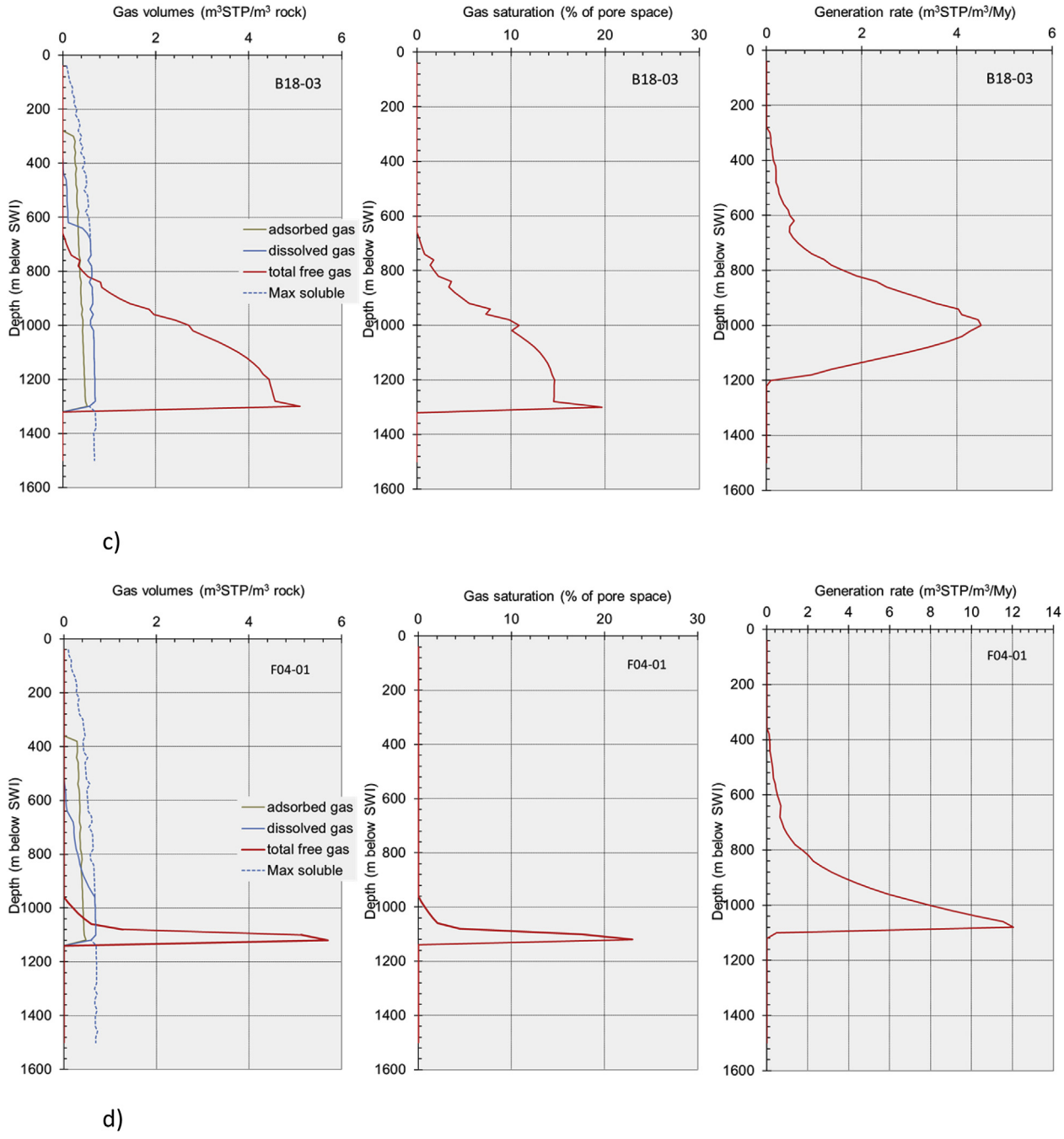

Fig. 17. (*continued*)

for the sample with 45% of sand at 416 m at B13-04). Fig. 21 further shows that the capillary seal capacity increases with depth in large part because of the decrease in pore-throat size and increase in gas density with depth. The variation in seal capacity at the same depth is directly related to the variation in pore-throat size at that depth. The change of capillary seal capacity with depth for the different seismostratigraphic sequences shows a number of interesting features (Fig. 21). Sequence S13 at about 400 m depth is the most shallow one of the SNS Delta and its variation in depth is minor. The capillary seal capacity of the S13 mudstone layers (sand content < 20%) at this relatively shallow depth is still 13-16 m. The seal capacities for the mudstones in sequences S5 and S6 are available over a relatively large depth interval from 500 to 900 m. They show the increase in capillary seal capacity with depth within a single delta sequence.

The grain-size based calculated properties of the intra-delta seals are lab scale properties. In order to evaluate the applicability of the calculated values on larger scale, the heights of the gas columns were compared with those calculated from measured WFT pressures and with other indicators of gas column heights, such as the heights of gas occurrences detected from cross-overs of neutron and density logs. At 5 well locations the available data allowed such a comparison (A12-03, A18-02, B13-03, B17-06, F02-06). The comparison indicated that the grainsize-based method to calculate capillary seal capacity provided pretty good estimates of maximum hydrocarbon column height for conditions at wells A12-03 and A18-02 and for part of the sampled seals at B10-03 and B17-06, while the dynamic charging conditions of the shallow gas reservoir tapped by F02-06 may have turned the mudstone layer into a permeability seal (Ten Veen et al., 2013). Below we first describe the F02-06 case followed by examples of comparison at well A12-03 and well A18-02.

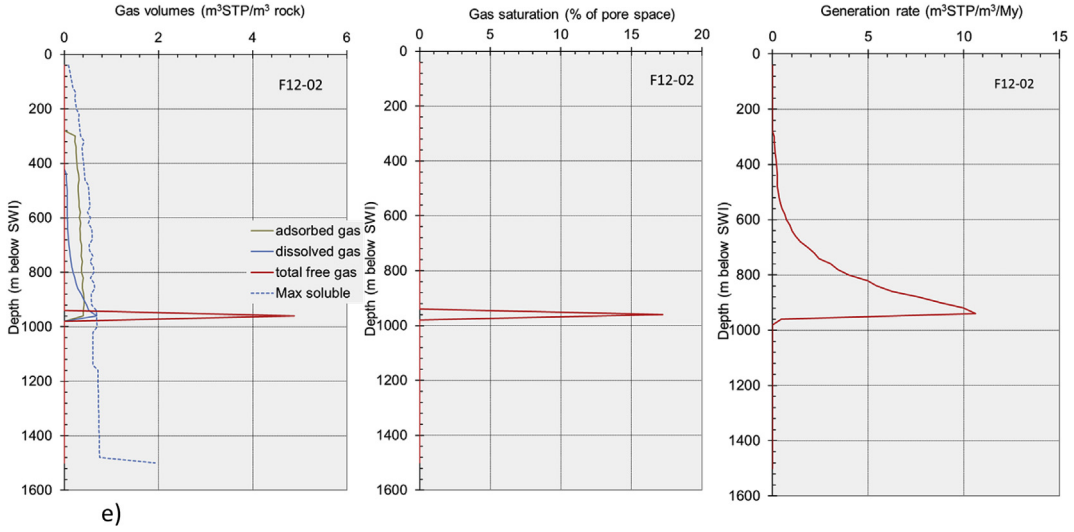

Fig. 17. (*continued*)

Well F02-06 runs through the crest of the HANP shallow gas field. The gas is trapped in a 4 way dip closed anticline. The reservoir consists of two distinct units: a good quality upper unit of 11–18 m containing 90% of the GIIP, and a poor quality lower unit with significant shales (F02-B-01 geological final well report, 2009; www.nlog.nl). The NPHI-RHOB cross-over at F02-06 indicates the presence of a gas column of 12 m immediately below the top seal. The grainsize-based calculated gas column height at F02-06 varies between 15 and 18 m at the depth of sampling between 641 and 671 m, which is well above the base of the seal at 690 m. Considering only the presence of gas in the upper reservoir suggests that the calculated hydrocarbon column height slightly overestimates the capillary seal capacity of the caprock. However, it seems that the hydrocarbon column extends into the low quality shale-rich reservoir until reaching a total gas column height of 40 m (Ten Veen et al., 2013). A fault cuts through the flank of the gas reservoir and it extends into the Hanze oil field reservoired in the overpressured Chalk on top of Zechstein salt structure. Oil and gas shows occur in the Paleogene mudrock overlying the oil field. It is unclear from public data whether the intercalated shales in the lower reservoir act as leaky intermediate seals or the top seal really holds a hydrocarbon column of 40 m. Assuming the latter case, Ten Veen et al. (2013) suggested that rapid fault related charging of the shallow gas trap may have increased the height of the gas column beyond capillary seal capacity, after which the top seal started to act as a permeability seal.

Well A12-03 is the discovery well of shallow gas field A12-FA. The well cuts through bright spots that are classified as stacked 4 way dip closures, overlying a salt structure and not fault bounded (Fig. 22). Application of the grain-sized based method using grain sizes derived

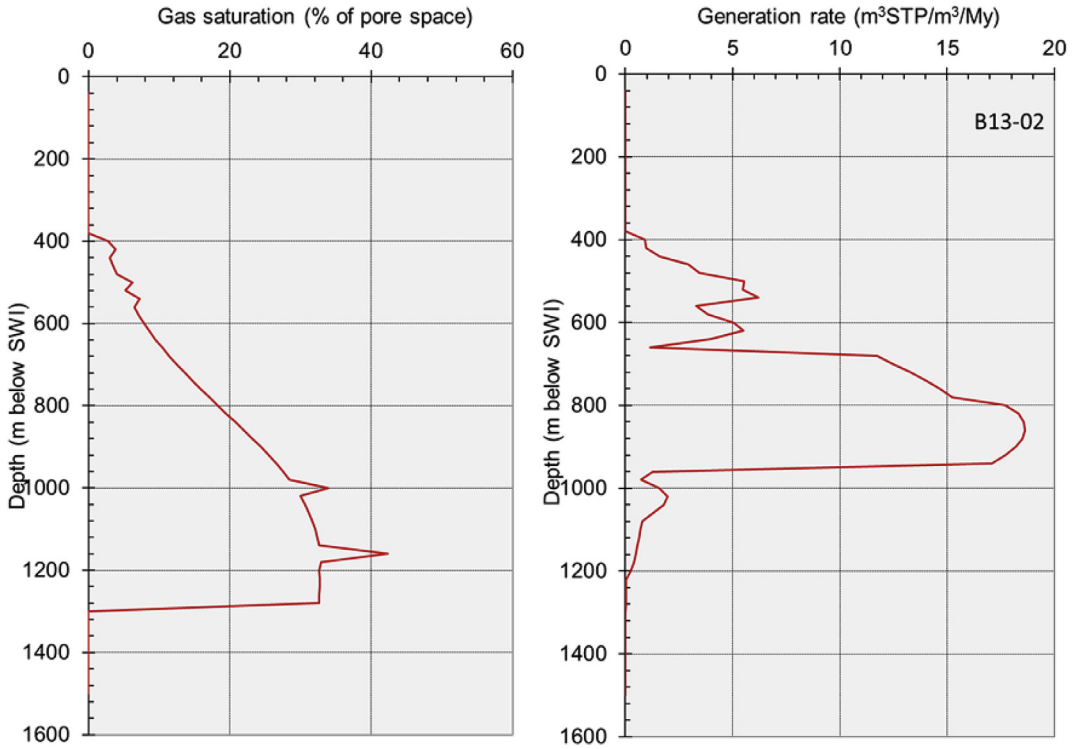

Fig. 18. Results of the simulation of microbial gas generation rate and gas saturation at well location B13-02, using the Thermal model of Biogenix for standard conditions.

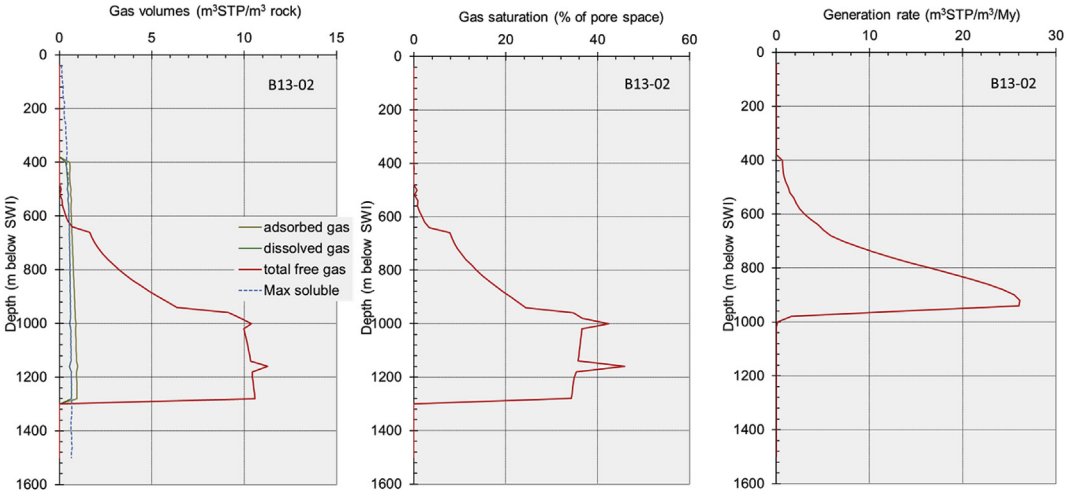

Fig. 19. Results of the simulation of microbial gas volumes, saturation and generation rate at well location B13-02, using the Hybrid model of Biogenix for TOC = 2% and otherwise standard conditions.

from core samples of the sealing mudstone at 431, 432 and 433 m depth at well A12-03 resulted in a calculated gas column height of 15 m (Fig. 22). This gas column height of 15 m exceeds the 10 m height of the NPHI-RHOB cross-over observed in the reservoir below the mudstone and the 9.5–10 m column height calculated from pressure data at well A12-03 (Fig. 22). Fig. 22 shows that well A12-03 is not cutting through the crest of the reservoir. As a consequence the NPHI-RHOB cross-over and the pressure-based gas column height underestimate the maximum seal capacity of the mudstone. The estimated hydrocarbon column height from the crest of the reservoir to the GWC derived from the cross-section shown in Fig. 22 would be about 1.5 times the hydrocarbon column height at well A12-03. Hence the mudstone seal holds a hydrocarbon column of 15 m, which corresponds nicely with the grain-size derived gas column height.

Well B13-03 is the discovery well of shallow gas field B13-FA. The well cuts through bright spots that are classified as stacked 4 way dip closures, overlying a salt structure and not fault bounded (Fig. 23). Table 1 shows that the gas column height of 14 m (sample depth 484 m) calculated with the grain-size method corresponds with both the pressure-derived and NPHI-RHOB cross-over derived magnitudes of column heights. The capillary seal capacity of the mudstone calculated by the grain-size method (12 m) at a depth of 339 m is higher than the NPHI-RHOB cross-over. The structure map of the top of the reservoir (Fig. 24) shows the position of the GWC and indicates that the hydrocarbon height from crest to GWC is only 6 m and that the trap is not filled to structural spill point. The identified sealing mudstone layer at the depth of 339 m is very thin (Table 1 and Fig. 23). A possible explanation of the difference between the calculated capillary seal capacity and hydrocarbon height may be that the thin mudstone layer and/or its lithological properties and therefore its seal capacity are not laterally continuous and may be less over the whole trap than the 12 m calculated from the grain-size of the sample taken at B13-03.

6.3. Leakage

Indicators of past or present vertical migration through the SNS delta deposits include: Christmas tree stacked bright spots (Figs. 22 and 23), drilled Christmas tree stacked shallow gas reservoirs (Fig. 23); bright spots along fault zones (Schroot and Schüttenhelm, 2003; Ten Veen et al., 2013); gas shows visible on logs (gas logs, NPHI-RHOB logs, Fig. 23). Ten Veen et al. (2013) found that many traps in the stacked bright spots are not filled to spill point as shown by comparison of the trap heights with gas column heights, either calculated using the grain size method or derived from cross-over plots or from WFT pressure data (Ten Veen et al., 2013). This suggests leakage through the mudstone top seals of these traps.

Indicators of leakage of gas from the delta deposits to the sea bed include very shallow seismic chimneys, pockmarks at the seabed and

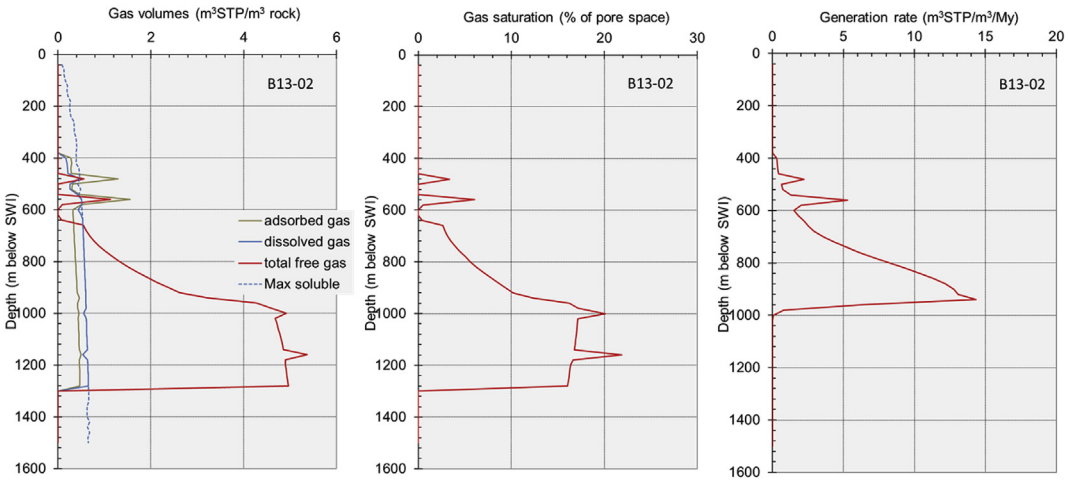

Fig. 20. Results of the simulation of microbial gas volumes, saturation and generation rate at well location B13-02, using the Hybrid model of Biogenix for variable TOC contents and otherwise standard conditions.

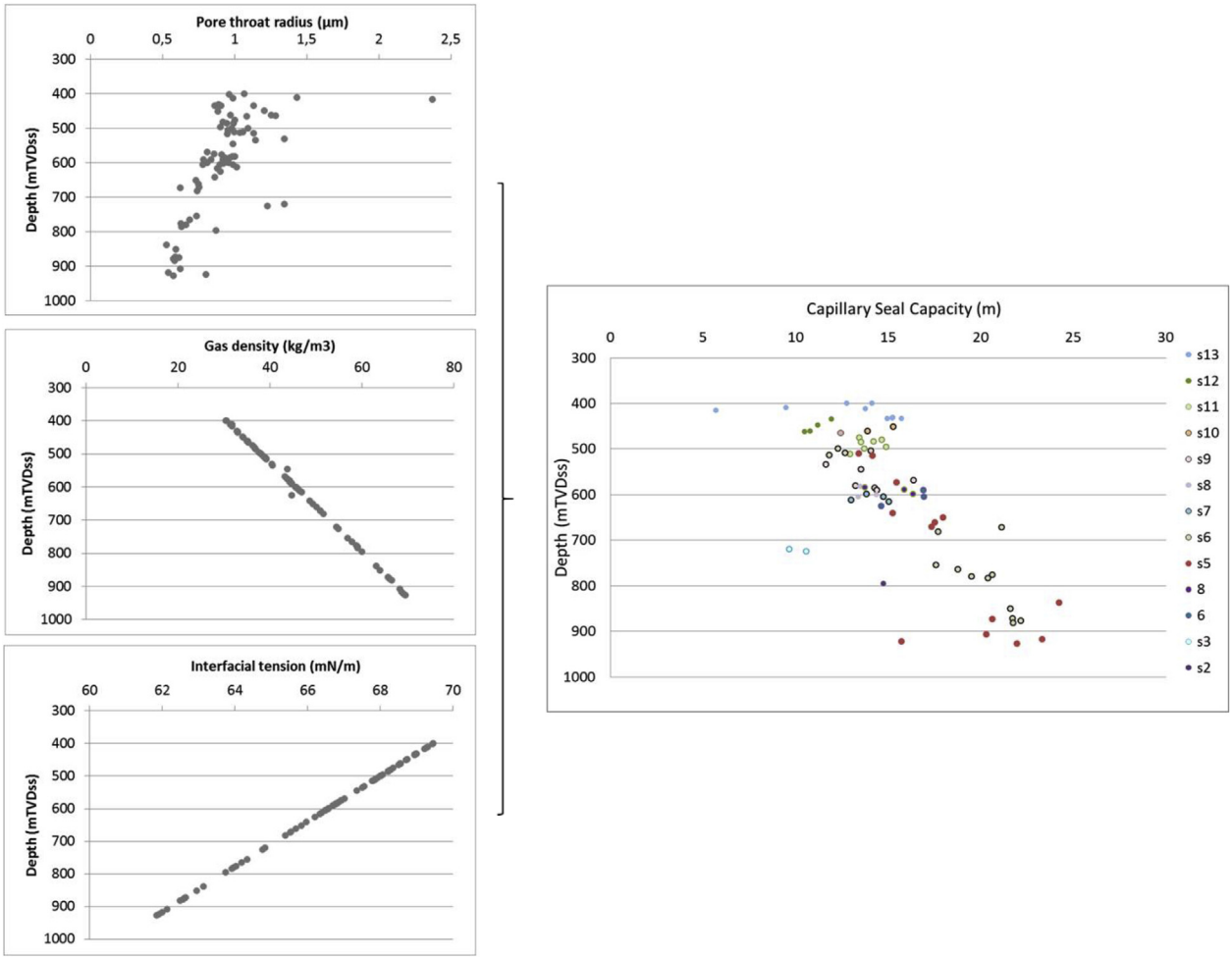

Fig. 21. Calculated capillary seal capacity of different delta sequences overlying shallow gas occurrences in the Southern North Sea Delta (Modified from Daza Cajigal, 2012 and Ten Veen et al., 2013).

gas plumes in the sea water. Indicators of very recent or ongoing leakage are the pockmarks at the sea bed and gas plumes in the sea water. Schroot and Schüttenhelm (2003) identified 3 pockmarks in the distribution area of the delta (in blocks A5, A11 and F10). The pockmark in A11 was studied later in more detail by Schroot et al. (2005).

There is one location where abundant ongoing gas leakage into the sea water has been reported and studied repeatedly (Schroot et al., 2005; Brussaard, 2013; Gentz, 2013; Mau et al., 2015; Römer et al., 2017; Urban et al., 2017). No pockmarks have been detected in association with these gas emissions (Schroot et al., 2005). This clear case of ongoing gas leakage occurs in the area of shallow gas field B13-FA (also called the 'the Dutch Dogger bank seep area' by Römer et al., 2017). Fig. 1 shows the location of shallow gas field in block B13. The cross-over of NPHI-RHOB logs at depths of less than 339 m at B13-03 (Fig. 23) shows the presence of gas in sediments overlying the thin mudstone seal. Schroot et al. (2005) presented evidence for the presence of gas pockets in near-surface sediments in the area based on sonar data and gas samples. Geochemical and carbon isotopic analysis of these gas samples show that the gas has a microbial signature. The presence of gas close to the sea bed was later confirmed by Römer et al. (2017) who identified gas pockets located at the boundary between the top of Late Pleistocene deposits and overlying fine-grained Holocene deposits by subbottom echosounder measurements. Several authors reported extensive gas plumes in the sea water in the area overlying shallow gas field B13-FA (Schroot et al., 2005; Brussaard, 2013; Gentz, 2013; Mau et al., 2015; Römer et al., 2017). Gas leaking from the shallow gas accumulations of B13-FA appears to be retained temporarily in the near surface sediments before being emitted into the sea water. Römer et al. (2017) mapped the gas emissions that were identified during 3 cruises in 2014, 2015 and 2016. They repeatedly detected 850 vents in the sea water within an area of about 8 km^2 and identified that 80% of these vents cluster close together in 5 distinct areas (the total area occupied by the 5 clusters is 15000 m^2). Römer et al. (2017) quantified the flow rates of methane released into the seawater for individual vents and for the cluster of vents based on measurements taken in 2014 and 2016. The average total flow of methane into the sea water from the total area occupied by the 5 clusters is 277 l/min or 51.5 Mol/min (Römer et al., 2017), which corresponds to a flux of about 1800 Mol/yr/m^2. The simulated gas generation rate in the B13 area varies between 5 m^3STP/Myr/m^3 to 15 m^3STP/Myr/m^3 (Fig. 20), corresponding to 0.223 to 0.669 mMol of gas generated per year per m^2 for a source rock thickness of 1 m. In order to sustain the flux of gas emission into the seawater entirely by ongoing microbial gas generation at present-day would require a drainage area of 2.7–8 km^2 for the assumed conditions. A total source rock thickness of 1 m in the delta in block B13 is probably quite conservative. In addition, gas generation has been active since a long time and has resulted in retention of the gas in the gas accumulations of B13-FA. Leakage from these accumulations probably contributes to the gas emission as well. The calculated drainage area should therefore be considered as maximum.

The question remains why those gas emissions occur at this B13 location today. A combination of conditions probably contribute to a natural explanation of the phenomenon: 1) gas field B13-FA is located

A12-03							
Seal Depth mTVDss	Sample Depth mTVDss	Sequence	Pressure measurement mTVDss	HC column height pressure-based From point of measurement (m)	From base seal m	HC column height grainsize-based m	NPHI – RHOB Cross over m
422.78 – 432.78	431;432;433	S13	433.27	9.5	10	15	10
515.75 – 526.75			530.27	20.5	24	-	22

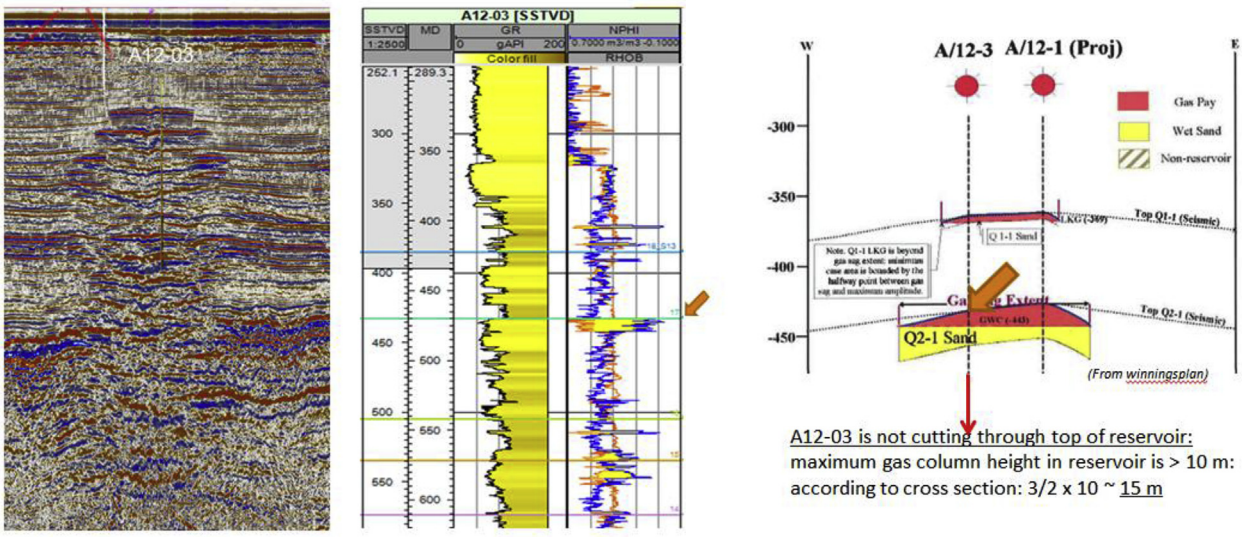

Fig. 22. From left to right: a) Seismic section showing location of well A12-03 cutting through stacked bright spots; b) Gamma ray, neutron (NPHI) and density (RHOB) logs; NPHI-RHOB cross-overs indicate presence of gas; arrow indicates location of mudstone samples; c) Cross-section showing geometry of top gas reservoir/ base mudstone seal; arrow indicates location of mudstone samples (Fig. 22 c derived from production plan A 12 field, retrieved from www.nlog.nl). The table presents gas column heights calculated using different methods.

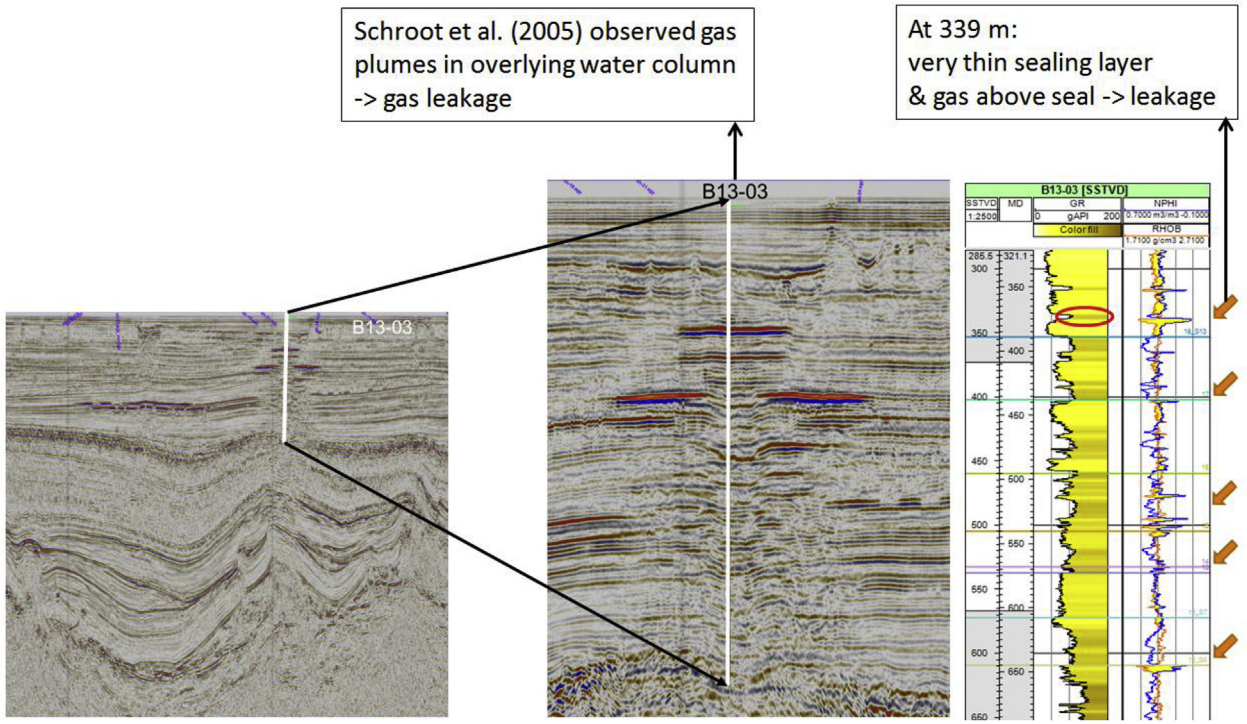

Fig. 23. From left to right: a) seismic sections showing location of well B13-03 cutting through stacked bright spots, overlying a salt structure; b) Gamma ray, neutron (NPHI) and density (RHOB) logs; NPHI-RHOB cross-overs indicate presence of gas; arrows indicate location of mudstone samples.

Table 1
Gas column heights calculated using different methods (well B13-03) (see Fig. 23 for location of mudstone samples).

Seal Depth mTVDss	Sample Depth mTVDss	Sequence	Pressure Depth mTVDss	HC column height P-based		HC column Grainsize-based (m)	NPHI-RHOB Cross over m
				From P Depth (m)	From Base Seal (m)		
B13-03							
336.4–339.9	339	Post S13	340.39	Inconclusive*		12	3
393.4–403.4	399	S13				13	1.5
481.4–494.4	484	S11	495.89	13.6	15	14	15
518.4–537.4	532	S9				12	
600.4–609.4	604	S7	609.89	10.4	10.9	15	5.5
600.4–609.4	604	S7	612.89	5.1	8.6	15	5.5

*uncertain water gradient.

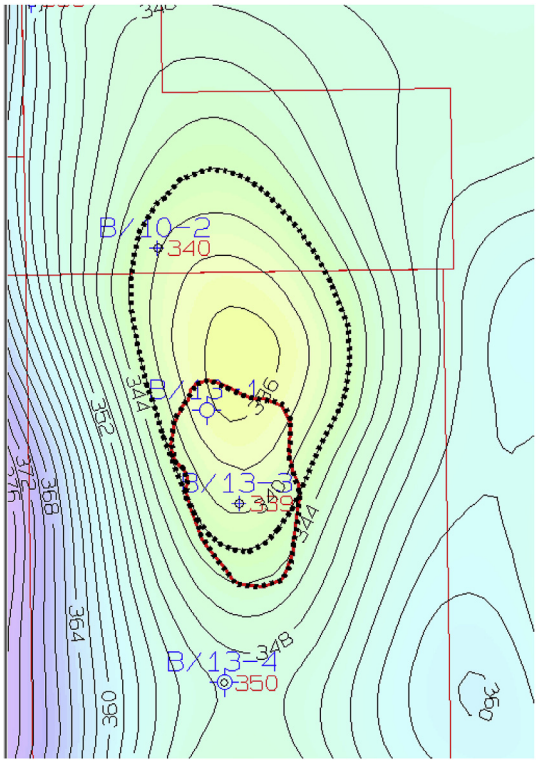

Fig. 24. Structure map of the top of a shallow gas reservoir belonging to field B13-FA (retrieved from www.nlog.nl; 9 October 2017). The depth of the crest of the reservoir identified at B13-03 is at 336 mSS and the GWC (black dotted line) at 342 mSS. The smaller red dotted line shows the amplitude extent at the reservoir. (For interpretation of the references to colour in this figure legend, the reader is referred to the Web version of this article.)

in the offshore B blocks where the base of the delta deposits reaches its greatest depth (Fig. 4) and it is located on top of a salt structure (Fig. 23): both circumstances enhance the thermal evolution and microbial gas generation in the delta deposits at B13-FA and its surroundings and an early start of the generation; 2) gas generation occurs already at shallow depths from a source with high percentage of TOC (4-5% TOC) (high % TOC observed in B13-03 at depth of 470 mMD and 553–554 mMD; see Figs. 10 and 20); 3) observed presence of organic matter in deposits overlying the delta sequences (e.g. lignites and woody remains in B10-02 and B13-01); 4) location of the B13-FA shallow gas field at the break location between the foreset and topset deposits in the S5 and S6 sequences (Stuart and Huuse, 2012; Ten Veen et al., 2013), and the regional focus of updip migration of gas through the foresets of the delta deposits towards this break location feeding the shallow gas field; and 5) last but not least the presence of a glacial valley overlying B13-03 (identified on seismic and shown in Fig. 3 in Kuhlmann et al., 2006b) and the leaky thin mudstone top seal (Fig. 23) just below the incised valley. The area of the B13-FA shallow gas field is not covered with 3D seismic; a possible relation of gas emission locations with fault related migration pathways could not be established on publicly available 2D seismic.

7. Discussion

The volumes of microbial gas generated in-situ in the delta are more than enough to explain published estimated volumes of shallow gas prospects in the delta. Identified seismic chimneys as well as bright spots associated with salt structures and/or faults feed the ongoing discussion whether or not also gas of deeper thermogenic origin has contributed to the shallow gas accumulations in the delta (Schroot and Schüttenhelm, 2003; Ten Veen et al., 2013, 2014). If so, it seems that the large volumes of in-situ generated microbial gas are dominant, as shown by the clear microbial signature of the gas.

Observed gas data did not allow to assess what microbial gas generation model (Hybrid or Thermal model of Biogenix) is the best model approach for the SNS delta. This is because it is generally not known whether observed data of mud gas, gas shows and gas accumulations in the SNS delta represent gas that was generated in-situ, gas that has migrated from greater depths or from elsewhere in the delta or a combination of in-situ and migrated gas.

The grainsize-based approach to estimate permeability and capillary seal capacity of intra-delta mudstones involves a number of assumptions and approximations that introduce uncertainty in the calculation results. Probably the main uncertainty is in the use of the equivalent grain size method of Nakayama and Sato (2002) to calculate pore throats (Ten Veen et al., 2013). Knowing that capillary seal capacity is a multi-scale property, and that mudstones also act as permeability seals and faulting and fracture zones crossing the mudstones influence the seal capacity, the grainsize-based method should be seen as a first phase of a more comprehensive approach to estimate preserved gas columns in bright spots in the SNS delta (Ten Veen et al., 2013; Verweij et al., 2014).

The current presence of shallow microbial gas accumulations in the SNS delta deposits is the final result of gas charging and leakage of stratigraphic and structural traps in the delta since the beginning of microbial gas generation, i.e. since about Early Pleistocene Calabrian times. This paper is based on observations of present-day properties, characteristics and seismic and log derived indicators of organic matter, gas, migration/leakage, traps and seals. The modelling of the burial and temperature history of the delta sequences and the 1D simulation of microbial gas generation take into account paleo conditions. A quantitative evaluation of the effects of stress and pressure changes on gas migration, entrapment and leakage was beyond the scope of the presented research projects. This also applies to the evaluation of the temporarily entrapment of gas and possible formation of gas hydrates below the permafrost during glacial conditions.

8. Conclusions

All essential elements (source, reservoir, seal, overburden) and processes (trap formation, generation-migration-accumulation) of a microbial gas system are present in the Dutch part of the SNS delta today. The microbial gas system in the delta is a highly dynamic system driven by ongoing burial of the delta sediments and ongoing microbial gas generation.

Source. The very high sedimentation rates during deposition of sequences S5-S13 of the SNS delta created favorable conditions for preservation of organic matter in the delta deposits. Organic matter is predominantly of land plant material with TOC values that vary from < 1 to 5% TOC, and mostly between 1 and 2% TOC. Coarser grained silty/sandy sediments deposited during the interglacials contain a higher amount of organic matter than the clayey/silty sediments deposited during glacials (e.g. in S5-S6).

Reservoir and seal. Interbedding of interglacial silty/sandy and glacial clayey/silty sediments of the delta provide reservoir/seal combinations. Interglacial sediments may act both as source rock and as carrier rock and/or reservoir rock. The calculated - vertical - permeability of the intra delta clay/silt seals (2.8E-20 m^2 to 1.1E-18 m^2; 2.8E-5 mD to 1.1E-3 mD) is several orders of magnitude smaller than the measured - horizontal - permeability of the carrier/reservoir layers ($2.5\,E-16\,m^2$ to $4.5\,E-12\,m^2$; 0.25 mD to 4560 mD). The calculated capillary seal capacity of the clay/silt layers varies between approximately 10 and 24 m. Both stratigraphic traps and salt movement related anticlinal traps were already created during deposition of the delta sequences.

Generation. Thermal simulations showed that optimal temperature conditions for microbial gas generation in the oldest and deepest buried SNS delta sequences started to develop in Early Pleistocene Calabrian times and continued to prevail until present-day. Simulations showed that generation of microbial gas at present-day starts already at depths of about 400 m, that is in the youngest sequences of the SNS delta. Simulated volumes of microbial gas generated in the Dutch part of the SNS delta (assuming TOC = 1% and a source rock thickness of 1 m) are more than enough to fill the published estimated total volumes of shallow gas prospects in the delta.

Migration and accumulation. The geometry of the E-W prograding delta sequences and the close interbedding of interglacial silty/sandy and glacial clayey/silty sediments focus gas migration updip through the foresets towards the topsets of the delta sequences, and ultimately into the anticlinal traps.

Leakage. Comparison of gas column heights derived from grain-size based calculations, cross plots of neutron and density logs and WFT pressure measurements, with trap heights derived from bright spots suggest that many traps in stacked bright spots are not filled to structural spill point. This suggests that filling of stacked reservoirs is not related to fill-spill migration, but rather to leakage through top seals. In absence of fault and fracture zones crossing the seals, such leakage is related to the capillary seal capacity and permeability of the top seals.

Simulated microbial gas generation from a drainage area of about 3–8 km^2 in the B13 area is enough to sustain observed average total flow of methane into the seawater in the area as published by Römer et al. (2017).

Acknowledgements

The presented research results were developed in the framework of the Joint industry Project “Shallow Gas” : executed by TNO, and in several in-house TNO projects. We thank TNO and the sponsors of the Joint Industry Project for their support: Dana Petroleum Netherlands B.V., Total E&P Nederland B.V., Oranje Nassau Energie B.V., Chevron Exploration and Production Netherlands B.V. (EBN). The two reviewers and the associated editor, dr. Robert Ondrak, are thanked for their constructive comments and suggestions that improved the paper.

References

Abdul Fattah, R., Verweij, J.M., Witmans, N., Ten Veen, J.H., 2012. Reconstruction of burial history, temperature, source rock maturity and hydrocarbon generation in the northwestern Dutch offshore. Netherlands J. Geosci.- Geologie en Mijnbouw 91 (4), 535–554.

Bernard, B.B., Brooks, J.M., Sackett, W.M., 1976. Natural gas seepage in the Gulf of Mexico. Earth Planet Sci. Lett. 31, 48–54.

Bernard, B.B., Brooks, J.M., Sacket, W.M., 1978. Light hydrocarbons in recent Texas continental shelf and slope sediments. J. Geophys. Res. 83, 4053–4061.

Bintanja, R., Van de Wal, R.S.W., 2008. North American ice-sheet dynamics and the onset of 100000 year glacial cycles. Nature 454, 869–872.

Bonté, D., Van Wees, J.-D., Verweij, J.M., 2012. Subsurface temperature of the onshore Netherlands: new temperature dataset and modelling. Netherlands J. Geosci.-Geologie en Mijnbouw 91 (4), 491–515.

Brussaard, C.P.D., 2013. CRUISE Report 64PE376 NIOZ Monitoring Leg1 ‘Methane Bubbles’ 2-8 September 2013. Royal Netherlands Institute for Sea Research (NIOZ).

Claypool, G.E., Magoon, L.B., Lorenson, ThD., Lillis, P.G., Kaplan, I.R., 2001. Natural gas in the Great Valley of California – geochemical characterization and petroleum systems. In: AAPG Annual Meeting 2001, Paper 8902.

Clayton, C., 1992. Source volumetrics of biogenic gas generation. In: Vially, R. (Ed.), Bacterial Gas. Editions Technip, Paris, pp. 191–202.

Clayton, C., 2010. Incorporation of biogenic gas generation into petroleum system models. In: Oral Presentation at the Geological Society of London meeting ‘Modelling Sedimentary Basins and their Petroleum Systems’, London, pp. 22–23 April 2010.

Daza Cajigal, V.A., 2012. The Evaluation of Sealing Properties of Mudstone Layers for Shallow Gas Accumulations in the Dutch Northern Offshore. MSc Thesis Faculty of Engineering, Politecnico di Torino, Italy (& Universidad Central de Venezuela, Facultad de Ingeniería, Caracas). pp. 81. http://saber.ucv.ve/bitstream/123456789/14380/1/Trabajo%20Especial%20de%20Grado.%20Valeria%20Daza.pdf.

Donders, T.H., Van Helmond, N.A.G.M., Verreussel, R., Munsterman, D., Ten Veen, J., Speijer, R.P., Weijers, J.W.H., Sangiorgi, F., Peterse, F., Reichart, G.-J., Sinnighe Damsté, J.S., Lourens, L., Kuhlman, G., Brinkhuis, H., 2018. Land-sea coupling of early Pleistocene glacial cycles in the southern North Sea exhibit dominant Northern Hemisphere forcing. Clim. Past 14 (3), 397–411. https://doi.org/10.5194/cp-14-397-2018.

Foschi, M., Cartwright, J.A., MacMinn, C.W., 2018. Sequential vertical gas charge into multilayered sequences controlled by central conduits. AAPG (Am. Assoc. Pet. Geol.) Bull. 102 (5), 855–883.

Gentz, T., 2013. Distribution and Fate of Methane Released from Submarine Sources; Results of Measurements Using an Improved *in Situ* Mass Spectrometer. PhD thesis. University of Bremen, Germany, pp. 173.

Govaerts, J., Beerten, K., Ten Veen, J., 2015. Numerical Simulation of Permafrost Depth in the Netherlands. Appendix 1 of Report OPERA-PU-TNO412pp. 44.

Guaipo Sarmiento, M.A., 2013. Modelling Biogenic Gas Generation in the Northern Dutch Offshore. MSc thesis. Faculty of Engineering, Politecnico di Torino, Italy, pp. 87. (& Universidad Central de Venezuela, Facultad de Ingeniería, Caracas). http://saber.ucv.ve/bitstream/123456789/14342/1/ThesisMariaGuaipo.pdf.

Head, I.M., Gray, N.D., Larter, S.R., 2014. Life in the slow lane; biogeochemistry of biodegraded petroleum containing reservoirs and implications for energy recovery and carbon management. Front. Microbiol. 5 (566), 23. https://doi.org/10.3389/fmicb.2014.00566.

Head, I.M., Jones, D.M., Larter, S.R., 2003. Biological activity in the deep subsurface and the origin of heavy oil. Nature 426, 344–352.

Hughes, A.L.C., Gyllencreutz, R., Lohne, Ø.S., Mangerud, J., Svendsen, J.I., 2016. The last Eurasian ice sheets – a chronological database and time-slice reconstruction, DATED-1. Boreas 45, 1–45.

Ingram, G.M., Urai, J.L., Naylor, M.A., 1997. Sealing processes and top seal assessment. In: In: Møller-Pedersen, P., Koestler, A.G. (Eds.), Hydrocarbon Seals: Importance for Exploration and Production, vol. 7. NPF Special Publication, pp. 165–174.

James, A.T., Burns, B.J., 1984. Microbial alteration of subsurface natural gas accumulations. AAPG Bull. 68 (8), 957–960.

Janszen, A., 2012. In: Tunnel Valleys: Genetic Models, Sedimentary Infill and 3D Architecture, vol. 220 PhD thesis Technical University Delft, the Netherlands978-94-6203-170-8, .

Judd, A., Hovland, M., 2009. Seabed Fluid Flow: the Impact on Geology, Biology and the Marine Environment. Cambridge University Press, pp. 492.

Katz, B.J., 2011. Microbial processes and natural gas accumulations. Open Geol. J. 5, 75–83.

Kombrink, H., Doornenbal, J.C., Duin, E.J.T., Den Dulk, M., Van Gessel, S.F., Ten Veen, J.H., Witmans, N., 2012a. New insights into the geological structure of The Netherlands; results of a detailed mapping project. Netherlands J. Geosci.-Geologie en Mijnbouw 91 (4), 419–446.

Kombrink, H., Ten Veen, J.H., Geluk, M.C., 2012b. Exploration in The Netherlands, 1987-2012. Netherlands J. Geosci.-Geologie en Mijnbouw 91 (4), 403–418.

Kuhlmann, G., De Boer, P.L., Pedersen, R.B., Wong, T.E., 2004. Provenance of Pliocene sediments and paleoenvironmental changes in the southern North Sea region using samariumneodymium provenance ages and clay mineralogy. Sediment. Geol. 171, 205–226.

Kuhlmann, G., Langereis, C.G., Munsterman, D., van Leeuwen, R.-J., Verreussel, R., Meulenkamp, J., Wong, ThE., 2006a. Chronostratigraphy of late Neogene sediments in the Southern North sea basin and paleoenvironmental interpretations. Palaeogeogr. Palaeoclimatol. Palaeoecol. 239, 426–455.

Kuhlmann, G., Langereis, C.G., Munsterman, D., Van Leeuwen, R.-J., Verreusel, R., Meulenkamp, J.E., Wong, ThE., 2006b. Integrated chronostratigraphy of the

Pliocene-Pleistocene interval and its relation to the regional stratigraphical stages in the southern North Sea region. Netherlands J. Geosci. – Geologie en Mijnbouw 85 (1), 19–35.
Kuhlmann, G., Wong, ThE., 2008. Pliocene paleoenvironment evolution as interpreted from 3D seismic data in the southern North Sea, Dutch offshore sector. Mar. Petrol. Geol. 25, 173–189.
Kurtev, K.D., Böker, U., Drews, M., Abrakasa, S., Aplin, A.C., 2012. Leaky top seals – evidence, rates and mechanisms. In: 3rd International Conference on Fault and Top Seals – from Characterization to Modelling, Montpellier, France, 1-3 October 2012, Extended Abstract.
Laban, C., 1999. Gaskraters in de Noordzee. In: Mens en Wetenschap, maart 1999. pp. 96–99 (in Dutch).
Laban, C., Van der Meer, J.M., 2011. Pleistocene glaciation in The Netherlands. In: In: Ehlers, J., Gibbard, P.L., Hughes, P.D. (Eds.), Developments in Quaternary Science, vol. 15. pp. 247–260 Amsterdam, The Netherlands.
Larter, S.R., Head, I.M., Huang, H., Bennett, B., Jones, M., Aplin, A.C., Murray, A., Erdmann, M., Wilhelms, A., Di Primio, R., 2005. Biodegradation, gas destruction and methane generation in deep subsurface petroleum reservoirs: an overview. In: Doré, A.G., Vining, B.A. (Eds.), Petroleum Geology: North-West Europe and Global Perspectives – Proceedings of the 6th Petroleum Geology Conference. Geological Society London, pp. 633–639.
Lee, J.R., Busschers, F.S., Sejrup, H.P., 2012. Pre-Weichselian Quaternary glaciations of the British Isles, The Netherlands, Norway and adjacent marine areas south of 68°N: implications for long-term ice sheet development in northern Europe. Quat. Sci. Rev. 44, 213–228.
Lorant, F., Largeau, C., Behar, F., De Cannière, P., 2008. Improved kinetic modeling of the early generation of CO2 from the Boom Clay kerogen. Implicaions for simulation of CO2 production upon disposal of hih activity nuclear waste. Org. Geochem. 39, 1294–1301.
Mau, S., Gentz, T., Körber, J.-H., Torres, M.E., Römer, M., Sahling, H., Wintersteller, P., Martinez, R., Schlüter, M., Helmke, E., 2015. Seasonal methane accumulation and release from a gas emission site in the central North Sea. Biogeosciences 12, 5261–5276.
Nakayama, N., Sato, D., 2002. Prediction of sealing capacity by the equivalent grain size method. In: Koestler, A.G., Hunsdale, R. (Eds.), Hydrocarbon Seal Quantification. NPF (Norwegian Petroleum Society), Amsterdam, pp. 51–60 Special Publication no.11, Elsevier Science B.V.
Noorbergen, L.J., Lourens, L.J., Munsterman, D.K., Verreussel, R.M.C.H., 2015. Stable isotope stratigraphy of the early Quaternary of borehole Noordwijk, southern North Sea. Quat. Int. 386, 148–157.
Nordgård Bolås, H.M., Hermanrud, Chr, Teige, G.M.G., 2005. Seal capacity estimation from subsurface pore pressures. Basin Res. 17, 583–599.
Overeem, I., Weltje, G.J., Bishop-Kay, C., Kroonenberg, S.B., 2001. The late cenozoic Eridanos delta system in the Southern North sea basin: a climate signal in sediment supply? Basin Res. 13 (3), 293–312.
Rollet, N., Logan, G.A., Kennard, J.M., O'Brien, P.E., Jones, A.T., Sexton, M., 2006. Characterisation and correlation of active hydrocarbon seepage using geophysical data sets: an example from the tropical, carbonate Yampi Shelf, Northwest Australia. Mar. Petrol. Geol. 23, 145–164.
Römer, M., Wenau, S., Mau, S., Veloso, M., Greinert, J., Schlüter, M., Bohrmann, G., 2017. Assessing marine gas emission activity and contribution to the atmospheric methane inventory: a multidisciplinary approach from the Dutch Dogger Bank seep area (North Sea). G-cubed 18. https://doi.org/10.1002/2017GC006995.
Schneider, F., Dubille, M., Montadert, L., 2016. Modeling of microbial gas generation: application to the Eastern Mediterranean "Biogenic Play". Geol. Acta 14, 403–417.
Schoell, M., 1988. Multiple origins of methane in the earth. Chem. Geol. 71, 1–10.
Schoell, M., 1983. Genetic characterization of natural gases. AAPG (Am. Assoc. Pet. Geol.) Bull. 67, 2225–2238.
Schroot, B.M., Klaver, G.T., Schüttenhelm, R.T.E., 2005. Surface and subsurface expressions of gas seepage to the seabed- examples from the Southern North Sea. Mar. Petrol. Geol. 22, 499–515.
Schroot, B.M., Schüttenhelm, R.T.E., 2003. Expressions of shallow gas in The Netherlands North Sea. Netherlands J. Geosci.-Geologie en Mijnbouw 82, 91–105.
Stuart, J.Y., Huuse, M., 2012. 3D seismic geomorphology of a large Plio-Pleistocene delta – 'Bright spots' and contourites in the Southern North Sea. Mar. Petrol. Geol. 38, 143–157.
Sweeney, R.E., 2001. Methanogenesis during biodegradation of petroleum in groundwater and oil/gas reservoirs. In: AAPG Annual Meeting 2001, Paper 6492.
Swint, P., 1999. Shallow Gas in the a and B Blocks; from Source to Reservoir. Internship report NAM report no. 199903000264. pp. 49.
Sylta, Ø., 2005. On the dynamics of capillary gas trapping: implications for the charging and leakage of gas reservoirs. In: Doré, A.G., Vining, B.A. (Eds.), Petroleum Geology: North West Europe and Global Perspectives – Proceedings of the 6th Petroleum Geological Conference. Geological Society, London, pp. 625–631.
Tambach, T.J., Van Leverink, D.J., Nepveu, M., Verweij, J.M., 2008. Calculation and Analysis of Geothermal Gradients: a Case Study for wells in the Dutch Offshore. TNO report 2008-U-R0273/A, Utrecht, The Netherlands. pp. 34.
Ten Veen, J., Verweij, H., Donders, T., Geel, K., De Bruin, G., Munsterman, D., Verreusel, R., Daza Cajigal, V., Harding, R., Cremer, H., 2013. Anatomy of the Cenozoic Eridanos Delta Hydrocarbon System. TNO report 2013 R10060. pp. 142 plus 10 appendices.
Ten Veen, J.H., Verweij, J.M., De Bruin, G., Donders, T., 2014. First steps toward maturing the shallow gas play – results of an exploration workflow. In: IPTC 17563. pp. 8.
Ter Voorde, M., Van Balen, R., Luijendijk, E., Kooi, H., 2014. Weichselian and Holocene climate history reflected in temperatures in the upper crust of The Netherlands. Netherlands J. Geosci.-Geologie en Mijnbouw 93 (3), 107–117.
Underschultz, J.R., Ellis, G., Hennig, A., Bekele, E., Otto, C., 2002. Estimating formation water salinity from wireline pressure data, case study in the Vulcan Sub-Basin: Western Australian Basins 3. In: Conference Proceedings, pp. 285–303.
Urban, P., Köser, K., Greinert, J., 2017. Processing of multibeam water column image data for automated bubble/seep detection and repeated mapping. Limnol Oceanogr. Meth. 15, 1–21.
Van den Boogaard, M., Gras, R., Hoetz, G., 2013. Shallow play in The Netherlands – derisked by seismic characterisation. In: 75th EAGE Conference & Exhibition Incorporating SPE EUROPEC 2013 London, UK, 10-13 June 2013, Extended abstract.
Van den Boogaard, M., Hoetz, H.L.J.H., 2012. Shallow gas play in The Netherlands takes off. In: 74th EAGE Conference & Exhibition Incorporating SPE EUROPEC 2012, Copenhagen, Denmark, 4-7 June 2012, 4 P, Extended abstract.
Verweij, H., De Bruin, G., Geel, K., 2016. Integrated approach to assess gas seepage systems. In: Keynote Lecture at GeofluidsVIII, 22-25 June 2016. China University of Geosciences, Wuhan, China.
Verweij, H., Nelskamp, S., Guaipo Sarmiento, M.A., 2013. Timing and distribution of biogenic gas generation in the shallow gas play in the Dutch offshore. In: 75th EAGE Conference & Exhibition Incorporating SPE EUROPEC 2013 London, UK, 10-13 June 2013, 4p, Extended abstract.
Verweij, J.M., 2003. Fluid Flow Systems Analysis on Geological Timescales in Onshore and Offshore Netherlands. With special reference to the Broad Fourteens Basin. PhD Thesis Vrije Universiteit Amsterdam_ Netherlands Research School of Sedimentary Geology Contribution No. 2003.09.05. 90-5986-035-7pp. 278.
Verweij, J.M., Daza Cajigal, V., De Bruin, G., Geel, K., 2014. Capillary Seal Capacity of Cenozoic mudstone Caprocks of shallow gas occurrences, Dutch offshore. In: Fourth EAGE Shale Workshop Shales: what Do They Have in Common?, 6-9 April 2014, Porto, Portugal, 5 P, Extended abstract.
Verweij, J.M., Kunakbayeva, G., Ghazaryan, L., 2015. Basin hydrodynamic system analysis – focus on vertical leakage and hydraulic continuity. In: First EAGE/TNO Workshop Basin Hydrodynamic Systems in Relation to Their Contained Resources, 6-8 May 2015, Utrecht, 4 P, Extended abstract.
Verweij, J.M., Nelskamp, S.N., 2014. Focus on shallow gas systems. In: First EAGE Workshop on Basin & Petroleum System Modeling. Advances of Basin and Petroleum Systems Modeling in Risk and Resource Assessment, 19-22 October 2014, Dubai, UAE, 5 P, Extended abstract.
Verweij, J.M., Vermooten, J.S.A., Simmelink, H.J., 2005. Variations in present-day temperatures and heat flow in onshore and offshore Netherlands. In: EAGE 67th Conference and Exhibition, Madrid, Spain, 13-16 June 2005, 4p, Extended abstract P201.
Whiticar, M.J., 1994. Correlation of natural gases with their sources. In: In: Magoon, L.B., Dow, W.G. (Eds.), The Petroleum System from Source to Trap, vol. 60. AAPG Memoir, pp. 261–283.
Whiticar, M.J., 1999. Carbon and hydrogen isotope systematics of bacterial formation and oxidation of methane. Chem. Geol. 161, 291–314.
Whiticar, M.J., Faber, E., Schoell, M., 1986. Biogenic methane formation in marine and freshwater environments: CO2 reduction vs. acetate fermentation – isotope evidence. Geochem. Cosmochim. Acta 50, 693–709.
Williams, J.D.O., Gent, C.M.A., 2015. Shallow gas Offshore Netherlands – the role of faulting and Implications for CO2 storage. In: Fourth International Conference on Fault and Top Seals, Alméria, Spain, 20-24 September 2015, 5 P, Extended abstract.
Yang, Y., Aplin, A.C., 2004. Definition and practical application of mudstone porosity-effective stress relationships. Petrol. Geosci. 10, 153–162.
Yang, Y., Aplin, A.C., 2010. A permeability-porosity relationship for mudstones. Mar. Petrol. Geol. 27, 1692–1697.
Zoth, G., Haenel, R., 1988. Chapter 10 appendix. In: Haenel, R., Rybach, R., Stegena, L. (Eds.), Handbook of Terrestrial Heat-flow Density Determination. Kluwer academic Publishers, Dordrecht, the Netherlands, pp. 449–466.